International Journal of Solids and Structures 225 (2021) 111060

Contents lists available at ScienceDirect

International Journal of Solids and Structures

journal homepage: www.elsevier.com/locate/ijsolstr

Stability of magnetic rings

Tuan Minh Hoang [a,b,c,*], David Vazquez Cortes [a]

[a] Okinawa Institute of Science and Technology Graduate University, Onna, Okinawa 904-0495, Japan
[b] Institute of Mechanics, VAST, 18 Hoang Quoc Viet, Hanoi, Viet Nam
[c] Graduate University of Science and Technology, VAST, 18 Hoang Quoc Viet, Hanoi, Viet Nam

ARTICLE INFO

Article history:
Received 9 December 2020
Received in revised form 13 April 2021
Accepted 19 April 2021
Available online 26 April 2021

Keywords:
Magnetic ring
Dipolar force
Compressive force
Stability
Permanent magnetization
Spherical particle
Multipole moment

ABSTRACT

Linear stability of magnetic rings consisting of permanently magnetized particles p of the same magnetization is studied. Employing Lagrange's approach and multipole moments, we determine the stability criterion in closed form. We then apply this criterion to characterize the stability for two scenarios in which the ring is i) compressed by dipolar loading due to a central point dipole and ii) compressed by mechanical loading. In contrast to previous works which show break up of magnetic rings under homogenous external magnetic field when instability occurs, we find that the ring does not break up when instability arises in both situations considered. However, the loading scenario decides instability modes via which the magnetic ring first loses its stability. For the first scenario, the ring deforms into planar but noncircular shapes via in-plane instability modes, regardless of ring sizes. For the other scenario, the ring deforms into planar but noncircular or nonplanar shapes via in-plane or out-of-plane instability modes for, respectively, small ring sizes or sufficiently large ring sizes. Finally, a simple experiment for the case of dipolar loading is proceeded and experimental results show good agreement with theoretical predictions.

1. Introduction

Structural instability has been a major concern for centuries in the design of all slender structures due to the load-capacity reduction and catastrophic failure and generally avoided in structural design. However, studies over the last decade have shifted toward the goal to harness such unstable phenomena for smart materials and structures (Hu and Burgueno, 2015). Of particular interest is instability of magnetic structures composed of permanently magnetized spherical particles. These structures are advantageous for many applications in magnetic materials, nanoscale electronics, medicine, and various other fields due to magnetic particles' capacity to be detected and manipulated using magnetic fields (Singamaneni et al., 2011).

The assembly of magnetic particles into magnetic rings and their stability play a vital role in many physical systems, i.e. designing switches for non-volatile random-access memory in magnetoelectronic application (Wei et al., 2009), explaining the aggregation processes in colloids (Wen et al., 1999), and understanding the origin of the Saturn's rings (van Putten, 2017). Moreover, the research of simple structures, like chains or rings, is essential since they can provide a starting point for understanding more complex structures. Stability of planar rings consisting of magnetized particles first attracted studies in ferrofluids. Previous works showed that planar rings consisting of superparamagnetic particles under the application of a homogeneous external magnetic field break up into chains when instability occurs, regardless whether the field directs perpendicular to the plane of the ring (Jund et al., 1995; Kun et al., 2001) or parallel to the plane of the ring (Kun et al., 2000). Subsequently, Danilov et al. (2012) examined stability of planar rings in a 2D monolayer consisting of magnetic dipolar particles under the influence of a homogeneous external magnetic field. They also showed that at the critical field strength, the rings either explode and form hexagonal lattice or break up into a chain when the field directs, respectively, perpendicular or parallel to the plane of the ring. Recently, Martinez-Pedrero et al. (2016) studied the formation and the dynamics of dipolar rings self-assembled from elliptical magnetic dipolar particles under homogeneous external magnetic field which directs parallel to the plane of the ring. They demonstrated the capability to manipulate the fragile magnetic rings and control their shape to perform functional tasks without ruptures or break up when instability occurs. Motived by this, we, in this paper, analyze stability of magnetic rings composed of permanently magnetized spherical

* Corresponding author at: Institute of Mechanics, VAST, 18 Hoang Quoc Viet, Hanoi, Viet Nam
E-mail address: tmhoang@imech.vast.vn (T.M. Hoang).

https://doi.org/10.1016/j.ijsolstr.2021.111060
0020-7683/

particles under external compressive loadings. We show how to deform the rings without ruptures or break up when instability occurs by utilizing compressive dipolar loading due to a point dipole placed at the center of the ring and oriented perpendicular to the plane of the ring, as illustrated in Fig. 2a. The theoretical predictions are then verified with a simple experiment of permanently magnetized spherical beads of millimeter sizes and we find that they are in good agreement with experimental results. The deformed shapes of our magnetic rings without rupture or break up, owing to high rate of shape changing, could be used to develop novel design concepts for actuators in MEMS or NEMS devices.

Stability of one dimensional magnetic structures has recently gained interests from the mechanics community, thanks to interesting works of Hall et al. (2013) and Vella et al. (2013). These authors first introduced the notion of effective bending stiffness for magnetic filaments composed of dipolar particles and demonstrated its advantage by analyzing stability of a vertical magnetic chain under its own weight, determining vibrating frequencies of a circular magnetic ring, and investigating the self-assembling process of a magnetic cylinder. In a related study, Boisson et al., 2015 examined linear dynamics of a chain of diametrically magnetized cylinders and determined the eigenfrequencies and associated eigenmodes from equation of motion. They showed a similar behavior between their magnetic system and an elastic beam. J. Schönke and E. Fried (Schönke and Fried, 2017) subsequently extended the work on stability of a vertical magnetic chain of dipolar particles under gravitational field to account for magnetic interactions between two coaxial vertical magnetic chains separated by a gap. Employing linear stability analysis, they determined the Hessian of the straight configuration in exact form which is used to yield the critical gap at which instability occurs. Their results also support the notion of effective bending stiffness for the system of two interacting magnetic chains. Motivated by the useful concept of effective bending stiffness, we, in this paper, also analyze stability of magnetic rings composed of permanently magnetized spherical particles subject to centrally mechanical loading, as demonstrated in Fig. 2b. We will determine the critical value of loading at which the ring loses its stability and investigate whether this value could be found from the application of concept of effective bending stiffness and classical results on stability of elastic rings subject to pressure.

The remainder of this paper is organized as follows. After formulating the problem in Section 2, we determine the general equilibrium and stability conditions in Section 3. Characterizations of our equilibrium configurations are given in Section 4 which is followed by their stability analysis in Section 5. Stability results for both scenarios are presented in Section 6. Experimental verification for a particular scenario in which the ring subject to a load induced by a central point dipole is reported in Section 7. A summary of our most important findings appears in Section 8.

2. Formulation

We consider a circular ring of $N \geq 4$ identical rigid spherical particles of diameter $d > 0$ and uniform permanent magnetization of strength $m > 0$. Letting $\boldsymbol{o}$ denote the center of the ring, we define a positively oriented orthonormal basis $\{\boldsymbol{e}_1, \boldsymbol{e}_2, \boldsymbol{e}_3\}$ such that the center $\boldsymbol{x}_i$ of each particle $i = 1, \dots, N$ lies in a plane with unit orientation $\boldsymbol{e}_3$. We measure lengths relative to d and energies relative to $\mu_0 m^2/4\pi d^3$, where μ_0 denotes the permeability of free space. Using $\boldsymbol{u}_i$ to denote the unit orientation of the dipole moment of particle $i = 1, 2, \dots, N$, introducing

$$\left.\begin{aligned} \boldsymbol{r}_i = \tfrac{\boldsymbol{x}_i - \boldsymbol{o}}{d}, \qquad r_i = |\boldsymbol{r}_i|, \qquad i = 1, \dots, N, \\ r_{ij} = \boldsymbol{r}_j - \boldsymbol{r}_i, \qquad r_{ij} = |\boldsymbol{r}_{ij}|, \qquad i,j = 1, \dots, N, \qquad i \neq j, \end{aligned}\right\} \tag{1}$$

and consulting (Jackson, 1999), we thus see that the dimensionless potential energy V of the ring can be expressed as

$$V = \sum_{1 \leqslant i < j \leqslant N} \sum \frac{1}{r_{ij}^3} \left(\boldsymbol{u}_i \cdot \boldsymbol{u}_j - \frac{3(\boldsymbol{r}_{ij} \cdot \boldsymbol{u}_i)(\boldsymbol{r}_{ij} \cdot \boldsymbol{u}_j)}{r_{ij}^2} \right). \tag{2}$$

We aim to understand how the configuration of the ring, as described by $\boldsymbol{u}_i$ and $\boldsymbol{r}_i, i = 1, \dots, N$, responds to placing a point dipole with strength M and orientation $\boldsymbol{e}_3$ at its center $\boldsymbol{o}$ and applying a force $-F\boldsymbol{r}_i/r_i$ to the center of each of its particles $i = 1, 2, \dots, N$. Since, for $M = 0$ and $F = 0$, the ring possesses reflection symmetry across the plane it occupies, we suppose, without loss of generality, that $M \geq 0$. The magnetic moment and mechanical forces applied to the ring are conservative and the total dimensionless potential energy W associated with these forces takes the form

$$W = -k \sum_{1 \leqslant i \leqslant N} \frac{1}{r_i^3} \left(\boldsymbol{u}_i \cdot \boldsymbol{e}_3 - \frac{3(\boldsymbol{r}_i \cdot \boldsymbol{e}_3)(\boldsymbol{r}_i \cdot \boldsymbol{u}_i)}{r_i^2} \right) + f \sum_{1 \leqslant i \leqslant N} r_i, \tag{3}$$

where the dimensionless parameters

$$k = \frac{M}{m} \qquad \text{and} \qquad f = \frac{F}{\mu_0 m^2/4\pi d^4} \tag{4}$$

measure the strengths, relative to the strength of the dipole–dipole interactions between each isolated pair of particles in the ring, of the external dipole moment and the mechanical forces exerted on each particle of the ring. Building on the work of Prokopieva et al. (2009), who showed that a circular ring of $N \geq 4$ identical magnetic particles is stable in the absence of loads, namely for $k = 0$ and $f = 0$ as illustrated in Fig. 1, we seek to characterize the stability of the system for the following scenarios:

- $k > 0, f = 0$: compressive dipolar loading by a central point dipole, as illustrated in Fig. 2a;
- $k = 0, f > 0$: compressive mechanical loading, as illustrated in Fig. 2b;

The total dimensionless potential energy of the system consisting of the ring of magnetic particles , which we emphasize may deviate from circular, the central point dipole, and the forces applied to the particles is simply the sum

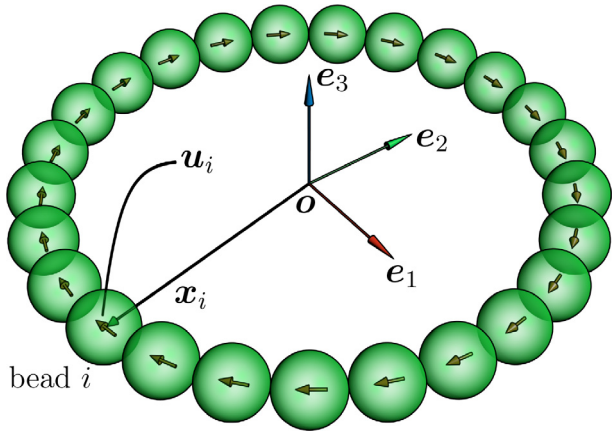

Fig. 1. A circular magnetic ring consisting of $N \geq 4$ identical rigid spherical particles , each of which has diameter d and possesses a uniform permanent magnetization with magnitude m. The position of the center of particle $i = 1, 2, \dots, N$ is denoted by $\boldsymbol{x}_i$ and the (unit) orientation of the dipole moment of that particle is denoted by $\boldsymbol{u}_i$. The center of the ring is denoted by $\boldsymbol{o}$ and the positively oriented orthonormal triad $\{\boldsymbol{e}_1, \boldsymbol{e}_2, \boldsymbol{e}_3\}$ is defined so that the centers of the particles lie in a plane spanned by $\boldsymbol{e}_1$ and $\boldsymbol{e}_2$.

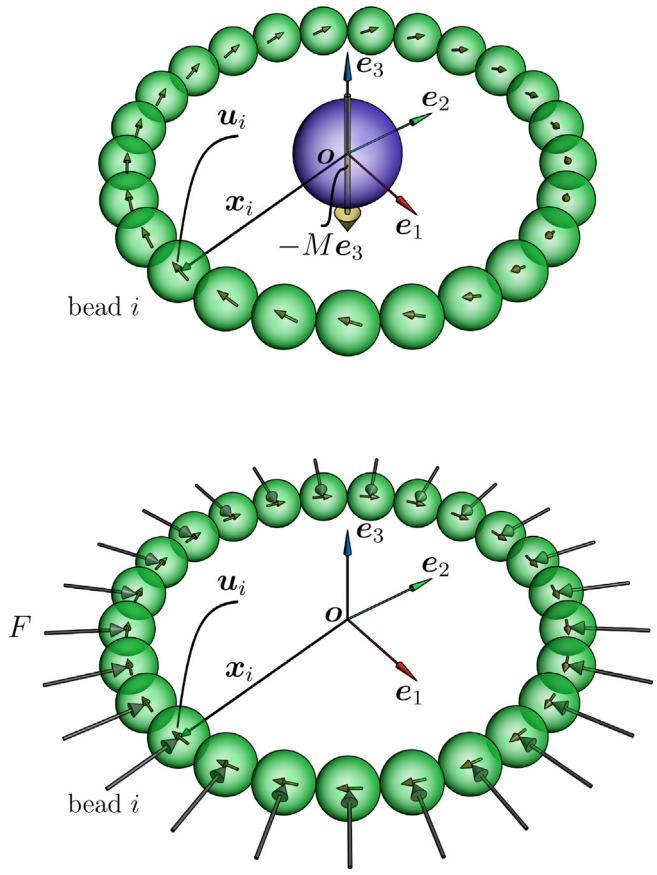

Fig. 2. A circular magnetic ring consisting of $N \geq 4$ identical rigid spherical particles whose centers lie in a plane spanned by $\boldsymbol{e}_1$ and $\boldsymbol{e}_2$ is subject to (a) a dipolar force due to a point dipole of magnetization strength M placing at its center $\boldsymbol{o}$ and directing antiparallel to the direction $\boldsymbol{e}_3$, (b) a compressive mechanical force of magnitude F applying to the center of each of its particles $i = 1, 2, \ldots, N$ and directing toward the center $\boldsymbol{o}$ of the ring.

$$E = V + W, \tag{5}$$

with V and W given by (2) and (3). Since $\boldsymbol{u}_i$ represents the unit orientation of the dipole moment of particle $i = 1, 2, \ldots, N$, we have the constraint

$$g_i \equiv \frac{1}{2}(|\boldsymbol{u}_i|^2 - 1) = 0, \qquad i = 1, \ldots, N. \tag{6}$$

Throughout our analysis, we require that adjacent particles remain in contact. Thus, introducing the convention $\boldsymbol{r}_{N+1} \equiv \boldsymbol{r}_1$, we impose the additional constraint

$$g_{N+i} \equiv \frac{1}{2}(|\boldsymbol{r}_{i+1} - \boldsymbol{r}_i|^2 - 1) = 0, \qquad i = 1, \ldots, N. \tag{7}$$

To characterize the stability of the system, we therefore introduce Lagrange multipliers $\lambda_i, i = 1, \ldots, 2N$, and consider the problem of determining the critical points of the augmented dimensionless total potential energy L defined by

$$L = E + \sum_{1 \leqslant i \leqslant N} (\lambda_i g_i + \lambda_{N+i} g_{N+i}). \tag{8}$$

3. Equilibrium and stability criteria

In deriving and analyzing the equilibrium and stability criteria for the system described in the previous section, we find it convenient and physically revealing to rewrite the components V and W of the augmented dimensionless total potential energy L defined in (8) as

$$V = -3 \sum_{1 \leqslant i < j \leqslant N} \sum \frac{\boldsymbol{Q}(\boldsymbol{r}_{ij}) \cdot (\boldsymbol{u}_i \otimes \boldsymbol{u}_j)}{r_{ij}^3} \qquad \text{and}$$

$$W = 3k \sum_{1 \leqslant i \leqslant N} \frac{\boldsymbol{Q}(\boldsymbol{r}_i) \cdot (\boldsymbol{e}_3 \otimes \boldsymbol{u}_i)}{r_i^3} + f \sum_{1 \leqslant i \leqslant N} r_i, \tag{9}$$

where $\boldsymbol{Q}$, the dimensionless quadrupole moment, is defined such that its value $\boldsymbol{Q}(\boldsymbol{r})$ at any vector $\boldsymbol{r} \neq \boldsymbol{0}$ is the second-order tensor

$$\boldsymbol{Q}(\boldsymbol{r}) = \frac{\boldsymbol{r} \otimes \boldsymbol{r}}{|\boldsymbol{r}|^2} - \frac{1}{3}\boldsymbol{I}. \tag{10}$$

We also take advantage of two higher-order counterparts of $\boldsymbol{Q}$, namely the dimensionless octupole and hexadecapole moments $\mathscr{O}$ and $\mathbb{H}$. For any vector $\boldsymbol{r} \neq \boldsymbol{0}$, the values $\mathscr{O}(\boldsymbol{r})$ and $\mathbb{H}(\boldsymbol{r})$ of $\mathscr{O}$ and $\mathbb{H}$ are respectively third- and fourth-order tensors that can be defined by transformation rules dictating how they operate on lower-order tensorial objects. For what follows, it is necessary to show how $\mathscr{O}(\boldsymbol{r})$ transforms second-order tensors into vectors and vectors into second-order tensors but is sufficient to show how $\mathbb{H}(\boldsymbol{r})$ transforms second-order tensors into second-order tensors. Specifically, given a second-order tensor $\boldsymbol{A}$ and a vector $\boldsymbol{v}$, $\mathscr{O}(\boldsymbol{r})\boldsymbol{A}$ is the vector defined such that

$$\mathscr{O}(\boldsymbol{r})\boldsymbol{A} = \frac{\boldsymbol{r} \cdot \boldsymbol{A}\boldsymbol{r}}{|\boldsymbol{r}|^2}\frac{\boldsymbol{r}}{|\boldsymbol{r}|} - \frac{1}{5}\frac{\boldsymbol{A}\boldsymbol{r} + \boldsymbol{A}^\top\boldsymbol{r} + (\mathrm{tr}\quad \boldsymbol{A})\boldsymbol{r}}{|\boldsymbol{r}|} \tag{11}$$

and $\mathscr{O}(\boldsymbol{r})\boldsymbol{v}$ is the second-order tensor defined such that

$$\mathscr{O}(\boldsymbol{r})\boldsymbol{v} = \frac{\boldsymbol{r} \cdot \boldsymbol{v}}{|\boldsymbol{r}|}\frac{\boldsymbol{r} \otimes \boldsymbol{r}}{|\boldsymbol{r}|^2} - \frac{1}{5}\frac{\boldsymbol{r} \otimes \boldsymbol{v} + \boldsymbol{v} \otimes \boldsymbol{r} + (\boldsymbol{r} \cdot \boldsymbol{v})\boldsymbol{I}}{|\boldsymbol{r}|}, \tag{12}$$

whereas $\mathbb{H}(\boldsymbol{r})\boldsymbol{A}$ is the second-order tensor defined such that

$$\mathbb{H}(\boldsymbol{r})\boldsymbol{A} = \frac{\boldsymbol{r} \cdot \boldsymbol{A}\boldsymbol{r}}{|\boldsymbol{r}|^2}\frac{\boldsymbol{r} \otimes \boldsymbol{r}}{|\boldsymbol{r}|^2} + \frac{1}{35}(\boldsymbol{A} + \boldsymbol{A}^\top + (\mathrm{tr}\boldsymbol{A})\boldsymbol{I}) - \frac{1}{7}\frac{(\boldsymbol{r} \cdot \boldsymbol{A}\boldsymbol{r})\boldsymbol{I} + (\boldsymbol{A} + \boldsymbol{A}^\top)(\boldsymbol{r} \otimes \boldsymbol{r}) + (\boldsymbol{r} \otimes \boldsymbol{r})(\boldsymbol{A} + \boldsymbol{A}^\top) + (\mathrm{tr}\boldsymbol{A})(\boldsymbol{r} \otimes \boldsymbol{r})}{|\boldsymbol{r}|^2}. \tag{13}$$

3.1. Equilibrium criteria

Any critical point of the augmented dimensionless potential energy L defined in (8) must be a solution $\boldsymbol{u}_i, \boldsymbol{r}_i, \lambda_i$, and $\lambda_{N+i}, i = 1, 2, \ldots, N$, of the system:

$$\left.\begin{aligned} \tfrac{\partial V}{\partial \boldsymbol{u}_i} + \tfrac{\partial W}{\partial \boldsymbol{u}_i} + \lambda_i \boldsymbol{u}_i &= \boldsymbol{0}, \\ \tfrac{\partial V}{\partial \boldsymbol{r}_i} + \tfrac{\partial W}{\partial \boldsymbol{r}_i} - \lambda_{N+i}(\boldsymbol{r}_{i+1} - \boldsymbol{r}_i) + \lambda_{N+i-1}(\boldsymbol{r}_i - \boldsymbol{r}_{i-1}) &= \boldsymbol{0}, \\ g_i &= 0, \\ g_{N+i} &= 0, \end{aligned}\right\} \qquad i = 1, \ldots, N. \tag{14}$$

Referring to the representations $(9)_1$ and $(9)_2$ of V and W and invoking the definitions (10) and (11) of the dimensionless quadrupole and octupole moment densities $\boldsymbol{Q}$ and $\mathscr{O}$, we find that the partial derivatives entering $(14)_1$ and $(14)_2$ can be expressed as

$$\left.\begin{aligned} \tfrac{\partial V}{\partial \boldsymbol{u}_i} &= -3 \sum_{\substack{1 \leqslant j \leqslant N \\ j \neq i}} \frac{\boldsymbol{Q}(\boldsymbol{r}_{ij})\boldsymbol{u}_j}{r_{ij}^3}, \\ \tfrac{\partial W}{\partial \boldsymbol{u}_i} &= 3k\frac{\boldsymbol{Q}(\boldsymbol{r}_i)\boldsymbol{e}_3}{r_i^3}, \end{aligned}\right\} \qquad i = 1, \ldots, N, \tag{15}$$

and

$$\left.\begin{aligned} \tfrac{\partial V}{\partial \boldsymbol{r}_i} &= -15 \sum_{\substack{1 \leqslant j \leqslant N \\ j \neq i}} \frac{\mathscr{O}(\boldsymbol{r}_{ij})(\boldsymbol{u}_i \otimes \boldsymbol{u}_j)}{r_{ij}^4}, \\ \tfrac{\partial W}{\partial \boldsymbol{r}_i} &= -15k\frac{\mathscr{O}(\boldsymbol{r}_i)(\boldsymbol{e}_3 \otimes \boldsymbol{u}_i)}{r_i^4} + f\frac{\boldsymbol{r}_i}{r_i}, \end{aligned}\right\} \qquad i = 1, \ldots, N, \tag{16}$$

A quick count shows that the system (14) consists of $8N$ scalar equations for the same number of unknown scalar quantities.

3.2. Stability criterion

Applying Theorem 2.8 of Avriel (1976) to the augmented dimensionless potential energy L defined in (8), we infer that a solution $\boldsymbol{u}_i, \boldsymbol{r}_i, \lambda_i$, and $\lambda_{N+i}, i = 1, \dots, N$, of the system (14) of equilibrium conditions is stable if the inequality

$$\sum_{1\leqslant i\neq j\leqslant N}\sum \left(\tfrac{\partial^2 V}{\partial \boldsymbol{u}_i\partial \boldsymbol{u}_j}\cdot(\delta\boldsymbol{u}_i\otimes\delta\boldsymbol{u}_j)+2\tfrac{\partial^2 V}{\partial \boldsymbol{u}_i\partial \boldsymbol{r}_j}\cdot(\delta\boldsymbol{u}_i\otimes\delta\boldsymbol{r}_j)+\tfrac{\partial^2 V}{\partial \boldsymbol{r}_i\partial \boldsymbol{r}_j}\cdot(\delta\boldsymbol{r}_i\otimes\delta\boldsymbol{r}_j)\right)$$
$$+\sum_{1\leqslant i\leqslant N}\left(2\tfrac{\partial^2 E}{\partial \boldsymbol{u}_i\partial \boldsymbol{r}_i}\cdot(\delta\boldsymbol{u}_i\otimes\delta\boldsymbol{r}_i)+\tfrac{\partial^2 E}{\partial \boldsymbol{r}_i^2}\cdot(\delta\boldsymbol{r}_i\otimes\delta\boldsymbol{r}_i)+\lambda_i|\delta\boldsymbol{u}_i|^2+\lambda_{N+i}|\delta\boldsymbol{r}_{i+1}-\delta\boldsymbol{r}_i|^2\right)\geqslant 0 \tag{17}$$

holds for all $\delta\boldsymbol{r}_i$ and $\delta\boldsymbol{u}_i, i = 1, \dots, N$, which, in compliance with the constraints (6) and (7), obey

$$\left.\begin{aligned}\boldsymbol{u}_i\cdot\delta\boldsymbol{u}_i&=0,\\(\boldsymbol{r}_{i+1}-\boldsymbol{r}_i)\cdot(\delta\boldsymbol{r}_{i+1}-\delta\boldsymbol{r}_i)&=0,\end{aligned}\right\}\qquad i=1,\dots,N, \tag{18}$$

where we have used the consequence $\delta\boldsymbol{r}_{N+1}\equiv\delta\boldsymbol{r}_1$ of the convention $\boldsymbol{r}_{N+1}\equiv\boldsymbol{r}_1$ introduced in connection with (7). In writing (17), we have made simplifications stemming from the respective consequences

$$\frac{\partial^2 W}{\partial \boldsymbol{r}_i\partial \boldsymbol{r}_j}=\frac{\partial^2 W}{\partial \boldsymbol{r}_i\partial \boldsymbol{u}_j}=\frac{\partial^2 W}{\partial \boldsymbol{u}_i\partial \boldsymbol{u}_j}=\boldsymbol{0},\qquad 1\leqslant i\neq j\leqslant N, \tag{19}$$

and

$$\frac{\partial^2 V}{\partial \boldsymbol{u}_i\partial \boldsymbol{u}_j}=\frac{\partial^2 W}{\partial \boldsymbol{u}_i\partial \boldsymbol{u}_j}=\boldsymbol{0},\qquad i=j=1,\dots,N, \tag{20}$$

of $(9)_1$ and $(9)_2$. Additionally, we exploited of the quadratic nature of the constraints (6) and (7). Referring to the representation $(9)_1$ of V and invoking the definitions (10), (12), and (13) of the dimensionless quadrupole, octupole, and hexadecapole moment densities $\mathbf{Q}, \mathscr{O}$, and $\mathbb{H}$, we find that the partial derivatives entering the double sum on the first line of (17) can be expressed as

$$\left.\begin{aligned}\tfrac{\partial^2 V}{\partial \boldsymbol{u}_i\partial \boldsymbol{u}_j}&=-3\tfrac{\mathbf{Q}(\boldsymbol{r}_{ij})}{r_{ij}^3},\\ \tfrac{\partial^2 V}{\partial \boldsymbol{r}_i\partial \boldsymbol{u}_j}&=-15\tfrac{\mathscr{O}(\boldsymbol{r}_{ij})\boldsymbol{u}_i}{r_{ij}^4},\\ \tfrac{\partial^2 V}{\partial \boldsymbol{r}_i\partial \boldsymbol{r}_j}&=105\tfrac{\mathbb{H}(\boldsymbol{r}_{ij})(\boldsymbol{u}_i\otimes\boldsymbol{u}_j)}{r_{ij}^5},\end{aligned}\right\}\qquad 1\leqslant i\neq j\leqslant N. \tag{21}$$

Similarly, recalling from (5) that $E = V + W$ and recalling the representations $(9)_1$ and $(9)_2$ of V and W and invoking the definitions (10), (12), and (13), we find that the partial derivatives entering the single sum on the second line of (17) can be expressed as

$$\left.\begin{aligned}\tfrac{\partial^2 E}{\partial \boldsymbol{u}_i\partial \boldsymbol{r}_i}&=-15\sum_{\substack{1\leqslant j\leqslant N\\ j\neq i}}\tfrac{\mathscr{O}(\boldsymbol{r}_{ij})\boldsymbol{u}_j}{r_{ij}^4}-15k\tfrac{\mathscr{O}(\boldsymbol{r}_i)\boldsymbol{e}_3}{r_i^4},\\ \tfrac{\partial^2 E}{\partial \boldsymbol{r}_i^2}&=-105\sum_{\substack{1\leqslant j\leqslant N\\ j\neq i}}\tfrac{\mathbb{H}(\boldsymbol{r}_{ij})(\boldsymbol{u}_i\otimes\boldsymbol{u}_j)}{r_{ij}^5}+105k\tfrac{\mathbb{H}(\boldsymbol{r}_i)(\boldsymbol{e}_3\otimes\boldsymbol{u}_i)}{r_i^5}+f\tfrac{\boldsymbol{P}(\boldsymbol{r}_i)}{r_i},\end{aligned}\right\}\qquad i=1,\dots,N, \tag{22}$$

where $\boldsymbol{P}$, the perpendicular projector, is the second-order tensor defined such that, for any vector $\boldsymbol{r}\neq\boldsymbol{0}$,

$$\boldsymbol{P}(\boldsymbol{r})=\boldsymbol{I}-\frac{\boldsymbol{r}\otimes\boldsymbol{r}}{|\boldsymbol{r}|^2}. \tag{23}$$

4. Circular base configurations with tilted dipole moments

Kun et al. (2001) showed that in the presence of a homogeneous external magnetic field oriented perpendicular to a circular ring of permanently magnetized spherical particles , the dipole orientations of those particles rotate out of plane until a critical threshold of field strength is attained and the ring ruptures. Motivated by that work, we seek solutions to the equilibrium Eqs. (14) wherein the ring remains circular but the dipole moments tilt out of plane in response to the field produced by the central point dipole. For this purpose, it is convenient to introduce the second-order tensor

$$\boldsymbol{R}=\cos(2\Pi_N)(\boldsymbol{e}_1\otimes\boldsymbol{e}_1+\boldsymbol{e}_2\otimes\boldsymbol{e}_2)$$
$$-\sin(2\Pi_N)(\boldsymbol{e}_1\otimes\boldsymbol{e}_2-\boldsymbol{e}_2\otimes\boldsymbol{e}_1)+\boldsymbol{e}_3\otimes\boldsymbol{e}_3,\qquad \Pi_N=\frac{\pi}{N}, \tag{24}$$

which rotates any vector about $\boldsymbol{e}_3$ by the angle $2\Pi_N$ between the centers of any adjacent pair of particles in the ring, and the associated cylindrical polar bases

$$\{\boldsymbol{\rho}_i,\boldsymbol{\varphi}_i,\boldsymbol{e}_3\}=\{\boldsymbol{R}^{i-1}\boldsymbol{e}_1,\boldsymbol{R}^{i-1}\boldsymbol{e}_2,\boldsymbol{e}_3\},\qquad i=1,\dots,N. \tag{25}$$

From (25), we see that

$$\left.\begin{aligned}\boldsymbol{\rho}_{i+1}\cdot\boldsymbol{\rho}_i&=\cos(2\Pi_N),\quad &|\boldsymbol{\rho}_{i+1}-\boldsymbol{\rho}_i|^2&=2(1-\cos(2\Pi_N))=4\sin^2\Pi_N,\\ \boldsymbol{\varphi}_{i+1}\cdot\boldsymbol{\varphi}_i&=\cos(2\Pi_N),\quad &\boldsymbol{\rho}_{i+1}\cdot\boldsymbol{\varphi}_i&=-\boldsymbol{\rho}_i\cdot\boldsymbol{\varphi}_{i+1}=\sin(2\Pi_N),\end{aligned}\right\}\qquad i=1,\dots,N, \tag{26}$$

where $\boldsymbol{\rho}_{N+1}\equiv\boldsymbol{\rho}_1$ and $\boldsymbol{\varphi}_{N+1}\equiv\boldsymbol{\varphi}_1$.

We assume that the dipole orientations are of the form

$$\boldsymbol{u}_i=\cos\theta\boldsymbol{\varphi}_i+\sin\theta\boldsymbol{e}_3,\qquad i=1,\dots,N, \tag{27}$$

where, to encompass the presence of tilt, θ satisfies

$$0<\theta\leqslant\frac{\pi}{2}. \tag{28}$$

Moreover, we assume that the ring placed so that

$$\boldsymbol{r}_i=\frac{\csc\Pi_N}{2}\boldsymbol{\rho}_i,\qquad i=1,\dots,N. \tag{29}$$

By $(26)_2$, (29) is consistent with the constraint (7). Also, by (25), $\boldsymbol{r}_1$ is aligned with $\boldsymbol{e}_1$ and, more generally, the index i increases upon viewing the ring from a vantage point above the plane it occupies and traversing it counterclockwise. For $\theta=\pi/2$, the dipoles are orthogonal to the plane of the ring and antiparallel to the direction of the central point dipole. Otherwise, for $0<\theta<\pi/2$, the dipole orientations are arranged with their tips directed clockwise and share the same out-of-plane component.

Substituting (27) and (29) into the general equilibrium conditions (14), we find that the tilt angle θ can take only two possible values consistent with (28), namely

$$\theta=\arcsin\left(\frac{8k}{3\sigma_3-\sigma_2}\right)=\theta_*\qquad\text{and}\qquad\theta=\frac{\pi}{2}, \tag{30}$$

where σ_2 and σ_3 denote the finite trigonometric sums

$$\sigma_2=\sum_{1\leqslant j\leqslant N-1}\csc(j\Pi_N)\qquad\text{and}\qquad\sigma_3=\sum_{1\leqslant j\leqslant N-1}\csc^3(j\Pi_N). \tag{31}$$

Since $3\csc^3(j\Pi_N)-\csc(j\Pi_N)\geq 2$ for $1\leqslant j\leqslant N-1$,

$$3\sigma_3-\sigma_2=\sum_{1\leqslant j\leqslant N-1}\csc^3(j\Pi_N)(3-\sin^2(j\Pi_N))\geq 2(N-1)\geq 6. \tag{32}$$

We thus see that the choice $\theta=\theta_*$ of the tilt angle in (30) is both viable and distinct from the alternative $\theta=\pi/2$ only if the dimensionless parameter k defined in $(4)_1$ satisfies

$$k<\frac{3\sigma_3-\sigma_2}{8}. \tag{33}$$

Granted that k satisfies (33) and that $\theta=\theta_*$, we find that the Lagrange multipliers needed to ensure that the constraints (6) and (7) are met are given by

$$\left.\begin{aligned}\lambda_i(\theta_*) &= (2\sigma_3-\sigma_2)\sin^3\Pi_N,\\ \lambda_{N+i}(\theta_*) &= -\tfrac{3}{2}\left(\tfrac{64k^2}{3\sigma_3-\sigma_2}+2\sigma_3-\sigma_2\right)\sin^3\Pi_N-\tfrac{f\csc\Pi_N}{2},\end{aligned}\right\}\quad i=1,\dots,N. \tag{34}$$

For the alternative choice $\theta=\pi/2$ of the tilt angle, we find, however, that (34) are overridden by

$$\left.\begin{aligned}\lambda_i\left(\tfrac{\pi}{2}\right) &= (8k-\sigma_3)\sin^3\Pi_N,\\ \lambda_{N+i}\left(\tfrac{\pi}{2}\right) &= -\tfrac{3}{2}(16k-\sigma_3)\sin^3\Pi_N-\tfrac{f\csc\Pi_N}{2},\end{aligned}\right\}\quad i=1,\dots,N. \tag{35}$$

If k violates (33), then (34) is irrelevant and only (35) applies. If, in particular, the central point dipole is absent, so that $k=0$, we see from (32) that $3\sigma_3>\sigma_2$. Thus, the argument of the arcsine in $(30)_1$ vanishes and $\theta_*=0$. As k increases from zero to a critical value k^{cr}, θ increases from zero to a critical value that can be found from $(30)_1$.

Hereafter, we stipulate that (33) holds and focus on exploring the stability of the circular base configuration for that choice of the tilt angle.

5. Linearized stability criterion for the nontrivial solution

To explore the stability of the ring in the circular base configuration with tilted dipole moments arranged according to (27), (29), and $(30)_1$, we consider perturbations of the general form

$$\left.\begin{aligned}\delta\boldsymbol{u}_i &= \alpha_i\boldsymbol{\rho}_i+\beta_i(\sin\theta\boldsymbol{\varphi}_i-\cos\theta\boldsymbol{e}_3),\\ \delta\boldsymbol{r}_i &= \chi_i\boldsymbol{\rho}_i+\upsilon_i\boldsymbol{\varphi}_i+\zeta_i\boldsymbol{e}_3,\end{aligned}\right\}\quad i=1,\dots,N, \tag{36}$$

in which the scalar coefficients obey

$$\alpha_i^2+\beta_i^2\ll 1,\qquad \chi_i^2+\upsilon_i^2+\zeta_i^2\ll 1,\qquad i=1,\dots,N. \tag{37}$$

With reference to (25) we find from (36) that, for $j\neq i$,

$$\begin{aligned}\delta\boldsymbol{u}_j &= (\alpha_j\cos(2(j-i)\Pi_N)-\beta_j\sin\theta\sin(2(j-i)\Pi_N))\boldsymbol{\rho}_i\\ &\quad+(\alpha_j\sin(2(j-i)\Pi_N)+\beta_j\sin\theta\cos(2(j-i)\Pi_N))\boldsymbol{\varphi}_i-\beta_j\cos\theta\boldsymbol{e}_3,\\ j&=1,\dots,N,\end{aligned} \tag{38}$$

and that

$$\begin{aligned}\delta\boldsymbol{r}_j &= (\chi_j\cos(2(j-i)\Pi_N)-\upsilon_j\sin(2(j-i)\Pi_N))\boldsymbol{\rho}_i\\ &\quad+(\chi_j\sin(2(j-i)\Pi_N)+\upsilon_j\cos(2(j-i)\Pi_N))\boldsymbol{\varphi}_i+\zeta_j\boldsymbol{e}_3,\\ j&=1,\dots,N.\end{aligned} \tag{39}$$

Although $(36)_1$ is consistent with the linearized consequence $(18)_1$ of the constraint (6), a supplemental condition is needed to ensure that $(36)_2$ is consistent with the linearized consequence $(18)_2$ of the remaining constraint (7). To determine that condition, we first observe that $(18)_2$ holds if and only if

$$\begin{aligned}\delta\boldsymbol{r}_{i+1}-\delta\boldsymbol{r}_i &= (\zeta_{i+1}-\zeta_i)\boldsymbol{e}_3+\frac{1}{2}(\chi_{i+1}-\chi_i-\tan\Pi_N(\upsilon_{i+1}+\upsilon_i))(\boldsymbol{\rho}_{i+1}+\boldsymbol{\rho}_i),\\ &\quad i=1,\dots,N,\end{aligned} \tag{40}$$

where $\chi_{N+1}\equiv\chi_1,\upsilon_{N+1}\equiv\upsilon_1$, and $\zeta_{N+1}\equiv\zeta_1$. Computing the scalar products with $\boldsymbol{\rho}_{i+1}$ and $\boldsymbol{\varphi}_{i+1}$ of the expression resulting from using $(36)_2$ in (40) and invoking $(26)_{1,3,4}$, we next find that $(36)_2$ meets the requirements of $(18)_2$ if and only if

$$\chi_{i+1}+\chi_i+\cot\Pi_N(\upsilon_{i+1}-\upsilon_i)=0,\qquad i=1,\dots,N. \tag{41}$$

We next use (27) with $\theta=\theta_*$, as defined in $(30)_1$, and (29) to evaluate the second-order partial derivatives (21) and (22) at the circular base configuration with tilted dipole moments, yielding (A.1) and (A.5), after which we insert $(30)_1$, (34), (36), (38), (39), and (A.1)–(A.5) into the stability criterion (17). With the additional assumption that the scalar coefficients of (36) admit Fourier decompositions of the particular form

$$\left.\begin{aligned}\alpha_i &= \mathrm{u}_1\cos(2q(i-1)\Pi_N),\\ \beta_i &= \mathrm{u}_2\sin(2q(i-1)\Pi_N),\\ \chi_i &= \mathrm{u}_3\cot\Pi_N\sin(2q(i-1)\Pi_N),\\ \upsilon_i &= \mathrm{u}_3\cot(q\Pi_N)\cos(2q(i-1)\Pi_N),\\ \zeta_i &= \mathrm{u}_4\cos(2q(i-1)\Pi_N),\end{aligned}\right\}\quad i=1,\dots,N. \tag{42}$$

where the amplitudes $\mathrm{u}_k,k=1,\dots,4$, are real numbers and a direct calculation confirms that $(42)_3$ and $(42)_4$ are consistent with (41), we arrive at the reduced stability criterion

$$\boldsymbol{u}\cdot\boldsymbol{H}\boldsymbol{u}=\begin{bmatrix}\mathrm{u}_1\\ \mathrm{u}_2\\ \mathrm{u}_3\\ \mathrm{u}_4\end{bmatrix}\cdot\begin{bmatrix}\mathrm{H}_{11}&\mathrm{H}_{12}&\mathrm{H}_{13}&\mathrm{H}_{14}\\ \mathrm{H}_{21}&\mathrm{H}_{22}&\mathrm{H}_{23}&\mathrm{H}_{24}\\ \mathrm{H}_{31}&\mathrm{H}_{32}&\mathrm{H}_{33}&\mathrm{H}_{34}\\ \mathrm{H}_{41}&\mathrm{H}_{42}&\mathrm{H}_{43}&\mathrm{H}_{44}\end{bmatrix}\begin{bmatrix}\mathrm{u}_1\\ \mathrm{u}_2\\ \mathrm{u}_3\\ \mathrm{u}_4\end{bmatrix}\geq 0, \tag{43}$$

where $\boldsymbol{H}$ is symmetric, so that

$$\begin{aligned}&\mathrm{H}_{21}=\mathrm{H}_{12},\quad \mathrm{H}_{31}=\mathrm{H}_{13},\quad \mathrm{H}_{32}=\mathrm{H}_{23},\quad \mathrm{H}_{41}\\ &\quad=\mathrm{H}_{14},\quad \mathrm{H}_{42}=\mathrm{H}_{24},\quad \mathrm{H}_{43}=\mathrm{H}_{34},\end{aligned} \tag{44}$$

and depends on the number N of particles in the ring, the loading parameters k and f, and the mode number q. Expressions for the entries of $\boldsymbol{H}$ are provided in A.2.

Denoting the necessarily real eigenvalues of $\boldsymbol{H}$ by $\eta_p,p=1,\dots,4$, we stipulate without loss of generality that they are ordered in accord with

$$\eta_1\leqslant\eta_2\leqslant\eta_3\leqslant\eta_4. \tag{45}$$

We denote the eigenvector (of unit magnitude) associated with η_p by $\boldsymbol{e}_p,p=1,\dots,4$. Furthermore, we introduce a Cartesian basis $\{\boldsymbol{i}_1,\boldsymbol{i}_2,\boldsymbol{i}_3,\boldsymbol{i}_4\}$ for $\mathbb{R}^4$ that implicitly determines the entries $\mathrm{u}_p=\boldsymbol{u}\cdot\boldsymbol{i}_p,p=1,\dots,4$, of $\boldsymbol{u}$ and $\mathrm{H}_{pq}=\boldsymbol{i}_p\cdot\boldsymbol{H}\boldsymbol{i}_q,p,q=1,\dots,4$, of $\boldsymbol{H}$.

In general, the mode number q ranges from $q=0$ to $q=n-1$, inclusive. However, since the first two mode numbers $q=0$ and $q=1$ correspond, respectively, to rigid body translations and rotations, which are of no physical interest in the present context, we require that $2\leqslant q\leqslant N-1$. Moreover, since the base configuration, as described by (27), (29), and $(30)_1$, is unchanged by application of any integer power of the rotation $\boldsymbol{R}$ defined in (24), it follows that q and $N-q$ are indistinguishable for each $q=1,\dots,N-1$. We may thus restrict the mode number according to

$$q=2,\dots,\lfloor\frac{N}{2}\rfloor, \tag{46}$$

where $\lfloor N/2\rfloor$ is the largest integer less than or equal to $N/2$.

For the base configuration of a ring of N particles subject to external loads characterized by k and f to be linearly stable with respect to perturbations involving mode number q, the least eigenvalue η_1 of $\boldsymbol{H}$ must satisfy $\eta_1>0$. Alternatively, the base configuration is linearly unstable if $\eta_1<0$. Moreover, if N and q are given and $\eta_1=0$ for any choice of the loading parameters k and f, then an instability occurs and the corresponding values of those parameters are called critical. Given $N\geq 4$ and q consistent with (46), we therefore solve the eigenvalue problem

$$\boldsymbol{H}\boldsymbol{e}=\eta\boldsymbol{e},\qquad |\boldsymbol{e}|=1, \tag{47}$$

with the objective of identifying values of k and f for which $\eta_1=0$. For any such value of k and f, we also determine the remaining eigenvalues η_2,η_3, and η_4 of $\boldsymbol{H}$ and, subsequently, the eigenvectors corresponding to all vanishing eigenvalues.

6. Stability results of a magnetic ring under dipolar and mechanical loadings

In this section, we determine critical values of k and f at which the smallest eigenvalue of $\boldsymbol{H}$ vanishes, dealing first with the case $f = 0$ of compressive dipolar loading by a central point dipole and then with the remaining case $k = 0$ of compressive mechanical loading. Although we consider all relevant modes $q = 2, \ldots, \lfloor N/2 \rfloor$, restrict attention to rings consisting of no more than $N = 50$ particles for practical reasons.

6.1. Dipolar loading

Given $N \geq 4$ and $q = 2, \ldots, \lfloor N/2 \rfloor$, we neglect mechanical loading by setting $f = 0$ and use an incremental approach to determine critical values k^{cr} of $k \geq 0$ by solving the eigenvalue problem (47) and subsequently checking the sign of the least eigenvalue η_1 of $\boldsymbol{H}$. Starting with $k = 0$, we augment the value of k by increments of $\Delta k = 10^{-3}$ until reaching the critical value $k = k^{\mathrm{cr}}$ at which $\eta_1 < 0$. After finding k^{cr}, we compute the associated critical eigenvector $\boldsymbol{e} = \boldsymbol{e}_1^{\mathrm{cr}}$, which determines the direction of the mode with respect to which the ring is least stable and, thus, tends to deform at the onset of instability.

Plots depicting the dependence of the critical value k^{cr} on the number N of particles in the ring for mode numbers $q = 2, 3, 4$, and $\lfloor N/2 \rfloor$ appear in Fig. 3. From these plots, we see that the lowest values of k^{cr} occur for mode number $q = 2$. This finding is reminiscent of results obtained, i.e., see (Carrier, 1947; Tadjbakhsh and Odeh, 1967; Flaherty et al., 1972; Giomi and Mahadevan, 2012; Chen and Fried, 2014; Biria and Fried, 2014; Hoang, 2019) for continuous ring-like objects subject to external pressure. From this similarity we infer that, before the ring becomes unstable, the field of the central point dipole generates a load that is effectively pressure-like.

Plots showing that the remaining eigenvalues η_2, η_3, and η_4 are positive at the critical value k^{cr} of k for any ring of up to $N = 50$ particles and mode number $q = 2$ are provided in Fig. 4. Qualitatively similar plots can be constructed for each of the other mode numbers. It is, thus, only necessary to find the eigenvector $\boldsymbol{e}_1^{\mathrm{cr}}$ associated with the vanishing of η_1 at k^{cr} for $q = 2$.

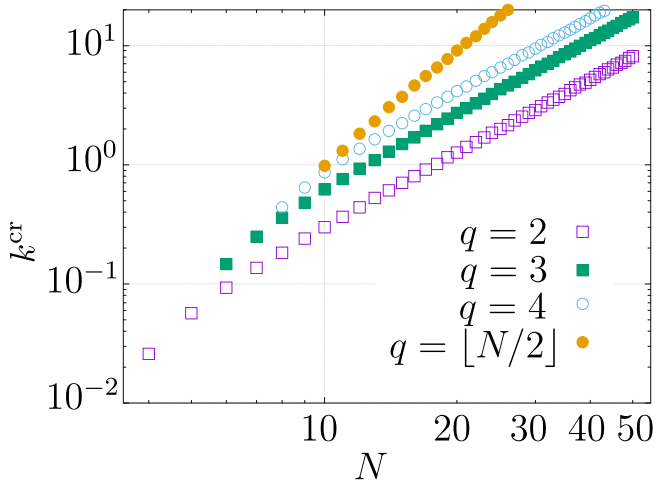

Fig. 3. Log–Log plots depicting the dependence of the critical values k^{cr} of k on the number N of particles of the ring in the absence of a mechanical load ($f = 0$) for mode numbers $q = 2, 3, 4$, and $\lfloor N/2 \rfloor$. The critical values k^{cr} are numerically determined by setting to zero the least eigenvalue of the symmetric 4×4 matrix $\boldsymbol{H}$ whose entries are analytically expressed as (A.6)–(A.15) in Appendix A.2. Since the critical values k^{cr} of k for a mode number $q = \lfloor N/2 \rfloor$ is the same as that for a mode number $q = 2, q = 3$, or $q = 4$ when $N = 4, 5, N = 6, 7$ or $N = 8, 9$, respectively, only the latter are shown.

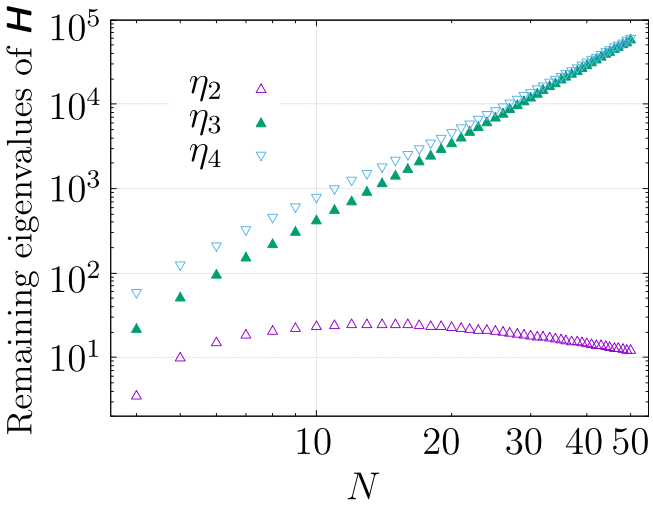

Fig. 4. Log–Log plots depicting the dependence of the remaining eigenvalues $\eta_p, p = 2, 3, 4$, of the symmetric 4×4 matrix $\boldsymbol{H}$, whose entries are analytically expressed as (A.16)–(A.25) in Appendix A.2 and the least eigenvalue η_1 vanishes at the critical values k^{cr} of k, on the number N of particles of the ring in the absence of a mechanical load ($f = 0$) for the second mode number $q = 2$.

Plots showing that, for $q = 2$, the ratios $|\boldsymbol{e}_1^{\mathrm{cr}} \cdot \boldsymbol{i}_2 / \boldsymbol{e}_1^{\mathrm{cr}} \cdot \boldsymbol{i}_1|$ and $|\boldsymbol{e}_1^{\mathrm{cr}} \cdot \boldsymbol{i}_4 / \boldsymbol{e}_1^{\mathrm{cr}} \cdot \boldsymbol{i}_3|$ decrease monotonically with N as N increases over the considered range appear in Fig. 5. For each N, $|\boldsymbol{e}_1^{\mathrm{cr}} \cdot \boldsymbol{i}_4 / \boldsymbol{e}_1^{\mathrm{cr}} \cdot \boldsymbol{i}_3|$ is smaller than $|\boldsymbol{e}_1^{\mathrm{cr}} \cdot \boldsymbol{i}_2 / \boldsymbol{e}_1^{\mathrm{cr}} \cdot \boldsymbol{i}_1|$ by at least an order of magnitude and decays somewhat more rapidly. Thus, we revisit the stability of the ring for $q = 2$ with reference to the assumed form (42) of the Fourier decompositions and two alternative simplifying assumptions:

- $\zeta_i = 0, i = 1 \ldots, N$;
- $\beta_i = 0$ and $\zeta_i = 0, i = 1 \ldots, N$.

For $\zeta_i = 0, i = 1 \ldots, N$, we find that the values of k^{cr} agree to three significant figures with those obtained previously (and used to generate the curve for $q = 2$ in Fig. 3). For $\beta_i = 0$ and $\zeta_i = 0, i = 1 \ldots, N$, we find in contrast that the values of k^{cr} are larger than those obtained previously. We therefore infer that the out-of-plane perturbation component $\zeta_i, i = 1 \ldots, N$, of positional perturbation $(36)_1$ has a negligible effect on the stability of the ring. This implies that the ring tends to deform in its plane, subverting the circular structure of dipole moments when instability occurs. In Section 7, we will consider the validity of this finding from an experimental perspective. At critical values k^{cr} of k, the least eigenvalue η_1 of $\boldsymbol{H}$ vanishes and the remaining eigenvalues $\eta_p, p = 2, 3, 4$, are positive and since the determinant of a matrix is the product of its eigenvalues, we infer that critical values k^{cr} are coincident with the vanishing of $\det \boldsymbol{H}$. Using (A.16)–(A.25) with $f = 0$ and the approximations (Vanderbei and Kolemen, 2007)

$$\sigma_2 \sim \frac{2 \log N}{\Pi_N} \quad \text{and} \quad \sigma_3 \sim \frac{2z}{\Pi_N^3}, \qquad z = \zeta(3) \approx 1.202. \tag{48}$$

we find that it is possible to determine a lengthy analytical expression k_∞^{cr} from the condition $\det \boldsymbol{H} = 0$. To dominant order in N as $N \to \infty$, that expression simplifies to

$$k_\infty^{\mathrm{cr}} \sim \frac{\sqrt{z(z + 1/6)}}{4\pi^2} N^2 + O(\log N), \qquad z = \zeta(3) \approx 1.202, \tag{49}$$

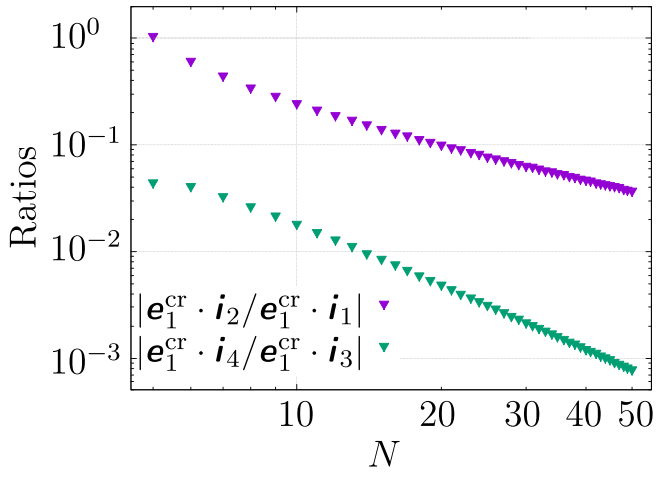

Fig. 5. Log–Log plots depicting the dependence of ratios $|\boldsymbol{e}_1^{\rm cr} \cdot \boldsymbol{i}_2/\boldsymbol{e}_1^{\rm cr} \cdot \boldsymbol{i}_1|$ and $|\boldsymbol{e}_1^{\rm cr} \cdot \boldsymbol{i}_4/\boldsymbol{e}_1^{\rm cr} \cdot \boldsymbol{i}_3|$ of the critical eigenvector $\boldsymbol{e}_1^{\rm cr}$, associated with the vanishing of the least eigenvalue η_1 of the symmetric 4×4 matrix $\boldsymbol{H}$ whose entries are analytically expressed as (A.16)–(A.25) in Appendix A.2 at the critical values $k^{\rm cr}$ of k, on the number N of particles of the ring in the absence of a mechanical load ($f = 0$) for the second mode. number $q = 2$.

which, in spite of its asymptotic stature, approximates $k^{\rm cr}$ with errors not exceeding 5% for $N \geq 13$, as illustrated in Fig. 6 and shown in Table 1 for some representative values of N. From the Fig. 6, we see that the relative error can be fitted to a straight line. Using the linear fit with the least square method, we find that the relative error decreases as $N^{-1.73}$. Combining this result with the expression of the relative error we infer, to dominant order in N as $N \to \infty$,

$$k_\infty^{\rm cr} \sim \frac{\sqrt{z(z+1/6)}}{4\pi^2} N^2 + O\left(N^{0.27}\right), \qquad z = \zeta(3) \approx 1.202. \tag{50}$$

Table 1
Numerical and asymptotic values for the critical value $k^{\rm cr}$ of k (determined by setting to zero the least eigenvalue of the symmetric 4×4 matrix $\boldsymbol{H}$ whose entries are analytically expressed as (A.16)–(A.25) in Appendix A.2 and from (49), respectively) and the relative error between them for representative numbers of particles N of the ring in the absence of a mechanical load ($f = 0$).

Number of particles N	Numerical value $k^{\rm cr}$	Asymptotic value $k_\infty^{\rm cr}$	Relative error (%) $\lvert k_\infty^{\rm cr} - k^{\rm cr}\rvert/k^{\rm cr}$
10	3.00	3.25	8.30
15	7.04	7.31	3.84
20	12.7	13.0	2.33
25	20.0	20.3	1.59
30	28.9	29.2	1.15
35	39.5	39.8	0.89
40	51.6	52.0	0.71
45	65.4	65.8	0.57
50	80.8	81.2	0.48

6.2. Mechanical loading

Given $N \geq 4$ and $q = 2, \ldots, \lfloor N/2 \rfloor$, we neglect magnetic loading by setting $k = 0$ and use an incremental approach to determine critical values $f^{\rm cr}$ of f by solving the eigenvalue problem (47) and subsequently checking the sign of the least eigenvalue η_1 of $\boldsymbol{H}$. Starting with $f = 0$, we augment $f^{\rm cr}$ by increments of $\Delta f = 10^{-4}$ until reaching the critical value $f = f^{\rm cr}$ at which $\eta_1 < 0$. After finding $f^{\rm cr}$, we compute the associated critical eigenvector $\boldsymbol{e}_1^{\rm cr}$, which gives the direction $\boldsymbol{e} = \boldsymbol{e}_1^{\rm cr}$ of the mode with respect to which the ring is least stable and, thus, tends to deform at the onset of instability.

Plots depicting the dependence of the critical value $f^{\rm cr}$ on the number $4 \leqslant N \leq 50$ of particles in the ring for mode numbers $q = 2, 3, 4$, and $\lfloor N/2 \rfloor$ appear in Fig. 7. From these plots, we see that the lowest values of $f^{\rm cr}$ occur for mode number $q = 2$. This finding is reminiscent of results for continuous ring-like objects subject to external pressure, i.e., see (Carrier, 1947; Tadjbakhsh and Odeh, 1967; Flaherty et al., 1972; Giomi and Mahadevan, 2012; Chen and Fried, 2014; Biria and Fried, 2014; Hoang, 2019).

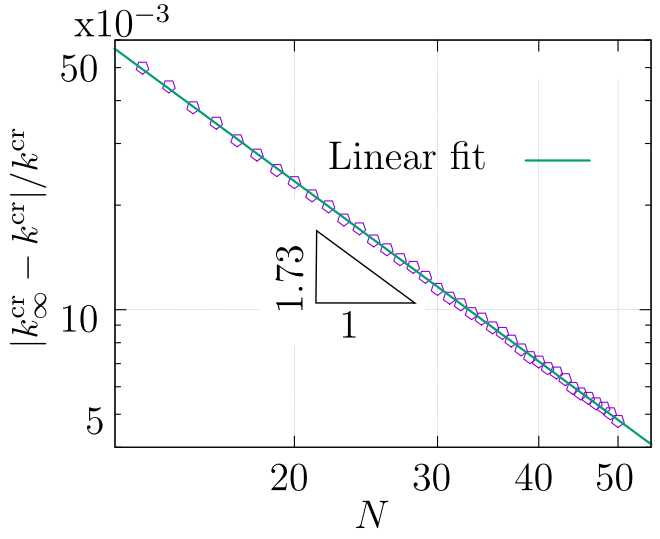

Fig. 6. Log–Log plots depicting the dependence of the relative error between the critical value $k^{\rm cr}$ (numerically determined by setting to zero the least eigenvalue of the symmetric 4×4 matrix $\boldsymbol{H}$ whose entries are analytically expressed as (A.16)–(A.25) in Appendix A.2 and corresponding to the curve for the second mode number $q = 2$ in Fig. 3) and its asymptotic value (49) on the number N of particles of the ring (points) in the absence of a mechanical load ($f = 0$). The linear fit (straight line), found by applying the least square method, reveals that the relative error $\sim N^{-1.73}$.

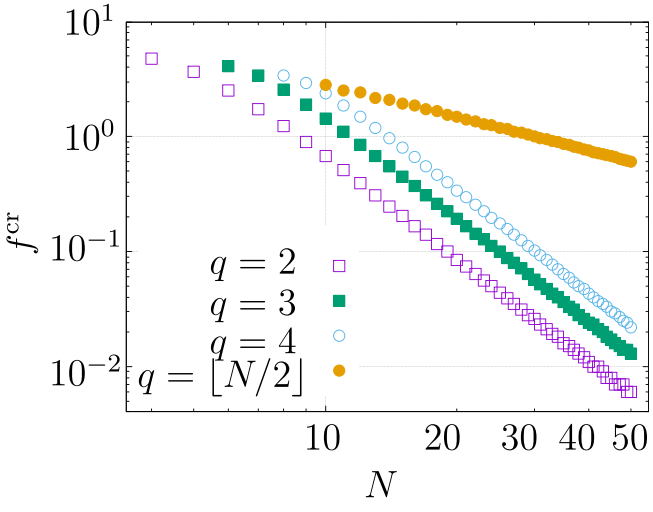

Fig. 7. Log–Log plots depicting the dependence of the critical values $f^{\rm cr}$ of f on the number N of particles of the ring in the absence of a dipole load ($k = 0$) for mode numbers $q = 2, 3, 4$, and $\lfloor N/2 \rfloor$. The critical values $f^{\rm cr}$ are numerically determined by setting to zero the least eigenvalue of the symmetric 4×4 matrix $\boldsymbol{H}$ whose entries are analytically expressed as (A.6)–(A.15) in Appendix A.2. Since the critical values $f^{\rm cr}$ of f for a mode number $q = \lfloor N/2 \rfloor$ is the same as that for a mode number $q = 2, q = 3$, or $q = 4$ when $N = 4, 5, N = 6, 7$ or $N = 8, 9$, respectively, only the latter are shown.

Plots showing that the remaining eigenvalues η_2, η_3, and η_4 are positive at the critical value f^{cr} of f for any ring of up to $N = 50$ particles and mode number $q = 2$ are provided in Fig. 8. Qualitatively similar plots can be constructed for each of the other mode numbers. It is, thus, only necessary to find the eigenvector $\boldsymbol{e}_1^{\mathrm{cr}}$ associated with the vanishing of η_1 at f^{cr} for $q = 2$.

For $q = 2$, determining the critical eigenvector $\boldsymbol{e}_1^{\mathrm{cr}}$ associated with the vanishing of η_1 at the critical values f^{cr} of f, we find that $\boldsymbol{e}_1^{\mathrm{cr}} \cdot \boldsymbol{i}_2 = \boldsymbol{e}_1^{\mathrm{cr}} \cdot \boldsymbol{i}_4 = 0$ for $N < 10$ and $\boldsymbol{e}_1^{\mathrm{cr}} \cdot \boldsymbol{i}_1 = \boldsymbol{e}_1^{\mathrm{cr}} \cdot \boldsymbol{i}_3 = 0$ for $N \geq 10$. Motivated by this finding and making reference to the assumed form (42) of the Fourier decompositions, we revisit the stability of the ring for $q = 2$ for two alternative simplifying cases:

- $\beta_i = 0$ and $\zeta_i = 0, i = 1 \ldots, N$;
- $\alpha_i = 0, \chi_i = 0$, and $\upsilon_i = 0, i = 1 \ldots, N$.

Analytical expressions for the critical values f^{cr} of f corresponding to these cases, which we denote by f_1^{cr} and f_2^{cr}, are provided in (A.29) and (A.32), respectively. Observing from those expressions that $f_1^{\mathrm{cr}} < f_2^{\mathrm{cr}}$ for $N < 10$ and $f_1^{\mathrm{cr}} > f_2^{\mathrm{cr}}$ for $N \geq 10$, we find that

$$f^{\mathrm{cr}} = \begin{cases} f_1^{\mathrm{cr}} & \text{for} \quad N < 10, \\ f_2^{\mathrm{cr}} & \text{for} \quad N \geq 10. \end{cases} \tag{51}$$

From this result, we infer that at the onset of instability sufficiently small rings tend to deform in-plane while sufficiently large rings tend to deform out-of-plane. Moreover, whereas the circular arrangement of the dipole moments is undermined during in-plane deformations, the underlying symmetry is preserved during out-of-plane deformations. To dominant order in N as $N \to \infty$, $(51)_2$ gives

$$f_\infty^{\mathrm{cr}} \sim 16(z + 1/6)\Pi_N^3 + O\left(\frac{\log N}{N^5}\right), \qquad z \approx 1.202, \tag{52}$$

which, in spite of its asymptotic stature, (52) approximates f^{cr} with errors not exceeding 1% for $N \geq 10$, as illustrated in Fig. 9 and shown in Table 2 for some representative values of N. As an alternative to the argument leading to (52), we next consider the feasibility of using a stability criterion derived by Hoang (2019) for a circular elastic ring, of uniform cross-section, that is subjected to a central loading of magnitude σ. The criterion in question involves the critical value of the "dimensionless pressure"

$$v = \frac{\sigma R^3}{EI}, \tag{53}$$

in which R is the radial distance between the center of the ring and the midline of its cross-section, E is the Young's modulus of the ring, and I is the cross-sectional area moment of inertia of the ring. Taking into account that, for a ring of N particles of diameter $d, R = d/2 \csc \Pi_N$, we may rewrite (53) as

$$v = \frac{\csc^3 \Pi_N}{8} \frac{\sigma d}{\mu_0 m^2/4\pi d^4} \frac{\mu_0 m^2/4\pi d^2}{EI}. \tag{54}$$

As the magnetic ring and the elastic ring are equipotent, we have $\sigma d = F$ and thus identify the middle ratio on the right-hand side of (54) with the magnitude of the dimensionless force $(16)_2$ specialized in accord with the assumed forms (27) and (29) for $\boldsymbol{u}_i$ and $\boldsymbol{r}_i, i = 1, \ldots, N$, and the requirement that $k = 0$, yielding

$$\frac{\sigma d}{\mu_0 m^2/4\pi d^4} = \left|\frac{\partial W}{\partial \boldsymbol{r}_i}\right| = f. \tag{55}$$

Additionally, we identify EI with the large N limit of the effective magnetic bending stiffness K_{eff} of a circular ring of uniformly magnetized spherical particles derived by Vella et al., 2013, which can be expressed as

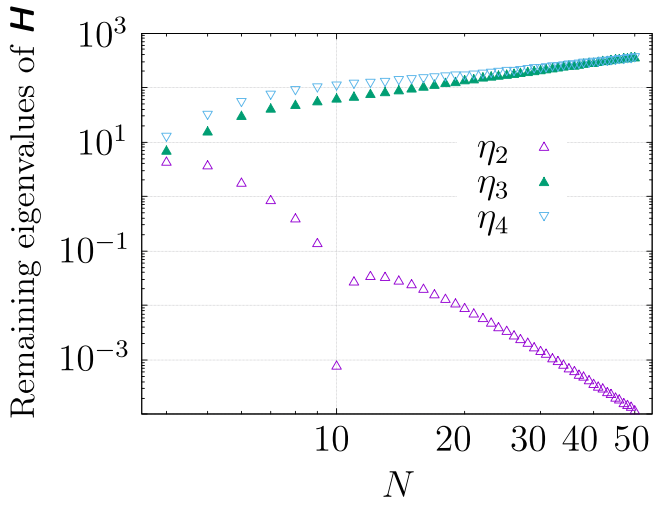

Fig. 8. Log–Log plots depicting the dependence of the remaining eigenvalues $\eta_p, p = 2, 3, 4$, of the symmetric 4×4 matrix $\boldsymbol{H}$, whose entries are analytically expressed as (A.16)–(A.25) in Appendix A.2 and the least eigenvalue η_1 vanishes at the critical values f^{cr} of f, on the number N of particles of the ring in the absence of a dipolar load ($k = 0$) for the second mode number $q = 2$.

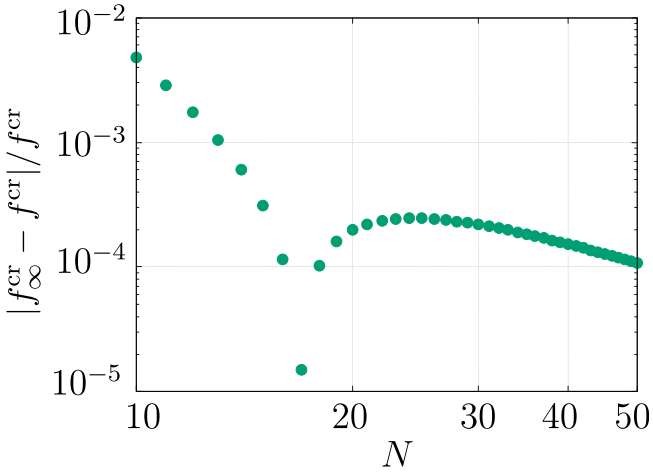

Fig. 9. Log–Log plots depicting the dependence of the relative error between the critical value f^{cr} (determined from the analytical expression (51) with (A.29) and (A.32) and corresponding to the curve for the second mode number $q = 2$ in Fig. 7) and its asymptotic value (52) on the number N of particles of the ring in the absence of a dipolar load ($k = 0$).

Table 2
Numerical and asymptotic values for the critical value f^{cr} of f (determined from the analytical expression (51) with (A.29) and (A.32) and from (52), respectively) and the relative error between them for representative numbers of particles N of the ring in the absence of a dipolar load ($k = 0$).

Number of particles N	Numerical value f^{cr}	Asymptotic value f_∞^{cr}	Relative error (%) $\lvert f_\infty^{\mathrm{cr}} - f^{\mathrm{cr}}\rvert/f^{\mathrm{cr}}$
10	675.8e−3	679.0e−3	4.8e−1
15	201.1e−3	201.1e−3	3.0e−2
20	84.89e−3	84.87e−3	1.9e−2
25	43.46e−3	43.45e−3	2.4e−2
30	25.15e−3	25.14e−3	2.1e−2
35	15.84e−3	15.83e−3	1.8e−2
40	10.61e−3	10.60e−3	1.5e−2
45	7.4e−3	7.4e−3	1.2e−2
50	5.4e−3	5.4e−3	1.0e−2

$$K_{\text{eff}} = \frac{\mu_0 m^2 (z + 1/6)}{8\pi d^2}, \tag{56}$$

where we have invoked the relation $B = 6\mu_0 m/\pi d^3$ for the flux density B of a spherical particle of uniform magnetization strength m and diameter d. It thus follows that

$$\frac{\mu_0 m^2/4\pi d^2}{EI} = \frac{\mu_0 m^2/4\pi d^2}{K_{\text{eff}}} = \frac{2}{z + 1/6}. \tag{57}$$

Using (55) and (57) in (54), invoking the relation (Hoang, 2019) for the critical value of the dimensionless pressure at which the elastic ring loses stability when

$$v = 4, \tag{58}$$

and solving for f we find that to dominant order in N as $N \to \infty$,

$$f_\infty^{\text{cr}} \sim 16(z + 1/6)\Pi_N^3, \qquad z \approx 1.202. \tag{59}$$

and is thus the result (52). Therefore, our results support the notion of an effective magnetic bending stiffness, first introduced by Hall et al. (2013) and Vella et al. (2013).

7. Experimental verification of the circular ring subject to a load induced by a central point dipole

7.1. Methods and experimental results

An experiment to study the instability of a magnetic ring under compression by a central magnetic dipole $\boldsymbol{m_0}$ fixed at the center of the ring was carried out by placing the magnetic ring and central magnetic dipole in a 3D printed case holder and recorded by a high speed camera. The case holder was designed in a computer assisted design software (*Freecad*), and printed by an Objet 500, 3D printer from *Stratasys*. The video was recorded with a phantom V641, color-high speed camera from *Vision research Inc*. Magnetic beads with diameters of $d = 5$mm and $D = 19.05$mm, and, magnetic strength of $B = 1.19T$ and $B_0 = 1.31T$ were used for the magnetic ring and central magnetic dipole respectively.

Fig. 10a shows a schematic cross section drawing of the experimental set up used to position the magnetic ring and align the central magnetic dipole. The case holder is designed to hold the center magnetic dipole in the plane of the magnetic ring, and to avoid its translational or rotational movements by activating the vacuum line observed in the figure.

In a first step, the magnetic ring is formed with 5 mm diameter magnetic beads and placed in the case holder. Concentric circles drawn from the position of the central magnetic dipole are used as guidelines for good centering of the ring. Before introducing the central magnetic dipole, a transparent acrylic plate with a conical shape machined in the bottom surface is used to hold the magnetic ring in place to avoid its interaction with the central magnetic dipole and keep its circular shape. Next, the central magnetic dipole is placed inside the case holder and aligned using a small, 5 mm diameter magnetic bead. Once the central magnetic dipole directs perpendicular to the plane of the magnetic ring, the vacuum line is activated and the small bead is removed. Finally, the acrylic plate is removed in a fast movement and the evolution of the magnetic ring recorded with the high speed camera as shown in Fig. 10b. The experiment was repeated for a wide range of number of beads (30 to 50) in the magnetic ring in order to determine the maximum number of beads for which the instability of the ring occurs.

The maximum number of beads in the ring for which the instability occurs is found to be 39 ± 2. Magnetic rings with 37–41 beads may or may not collapse to the central bead. This behavior is associated with the accuracy in the positioning and circularity of the magnetic ring. Fig. 11 shows frames from a video, recorded by a color-high speed camera after 10, 50 and 65 ms of the release of a ring with a number of 41 beads of 5 mm diameter. The behavior of rings that shows instability and deform to the central bead is very similar and independent of the number of magnetic beads. After releasing the magnetic ring it starts moving towards the center bead in one direction, and away from it in a perpendicular direction, forming an oval whose (mayor axis/minor axis) aspect ration increases with time. No out of plane movements were observed for the range of number of beads in the magnetic rings used in the experiments. The experiment was continued by reducing more the number of beads until 34. For rings with less than 37 beads the ring always deforms to the central bead.

7.2. Comparison with theoretical results

We first observe that the ring deforms in its plane subverting the circular structure of dipole moments when instability occurs. This thus confirms our theoretical result in Subsection 6.1 that the out-of-plane displacement of magnetic beads in the ring has a negligible role on the stability of the ring. We next find the maximum number of bead N_{max} at which instability occurs. From the relation between magnetic strength and its magnetization of a magnetic bead (Jackson, 1999),

$$\begin{aligned} B &= \tfrac{6\mu_0 m}{\pi d^3}, && \text{for the magnetic beads in the ring,} \\ B_0 &= \tfrac{6\mu_0 M}{\pi D^3}, && \text{for the magnetic central bead,} \end{aligned} \tag{60}$$

we have, from $(4)_1$,

$$k_0 = \frac{M}{m} = \left(\frac{D}{d}\right)^3 \left(\frac{B_0}{B}\right) = \left(\frac{19.05}{5}\right)^3 \left(\frac{1.31}{1.19}\right) \approx 60.88. \tag{61}$$

From the theoretical results as shown in Fig. 3, we find that $N_{max} = 43$ for the combination of bead diameters and magnetic strengths in our experiments because $k_0 > k^{\text{cr}}$ when $N \leqslant N_{max}$. If we assume the experiment result predicts an instability occurs when $N \leq 39$ then our theoretical prediction is in good agreement with the experiment, with the relative error being $(43 - 39)/39 \approx 10.3\%$. The discrepancy between our theory and experiment is probably due to the absence of frictional effects in our model.

8. Summary & discussion

We examined the linear stability analysis of magnetic rings of permanently magnetized particles subject to two different loading mechanisms: i) compressive dipolar loading due to a central point dipole and ii) compressive mechanical loading. Our model involves three parameters: the number of particles N, the dimensionless strength of the central dipole k and the mechanical force f exerted on each particle of the ring relative to the strength of the dipole–dipole interactions between each isolated pair of particles in the ring. Using quadrupole, octupole, and hexadecapole moments, we derived the stability criterion in explicit form. Due to the periodicity of our problem, we then employed discrete Fourier analysis to cast the stability condition in the definite quadratic form. Critical values of parameters at which instability occurs and the relevant instability modes are determined, respectively, by vanishing the least eigenvalue of the matrix of the quadratic form and obtaining the eigenvectors corresponding to all vanishing eigenvalues.

We find that the smallest critical values of loading parameters occur for the mode number $q = 2$, regardless of the loading mechanism considered. Our result suggests that before the ring becomes unstable, the field of the central point dipole generates a load that is effectively pressure-like, which is similar to the compressive

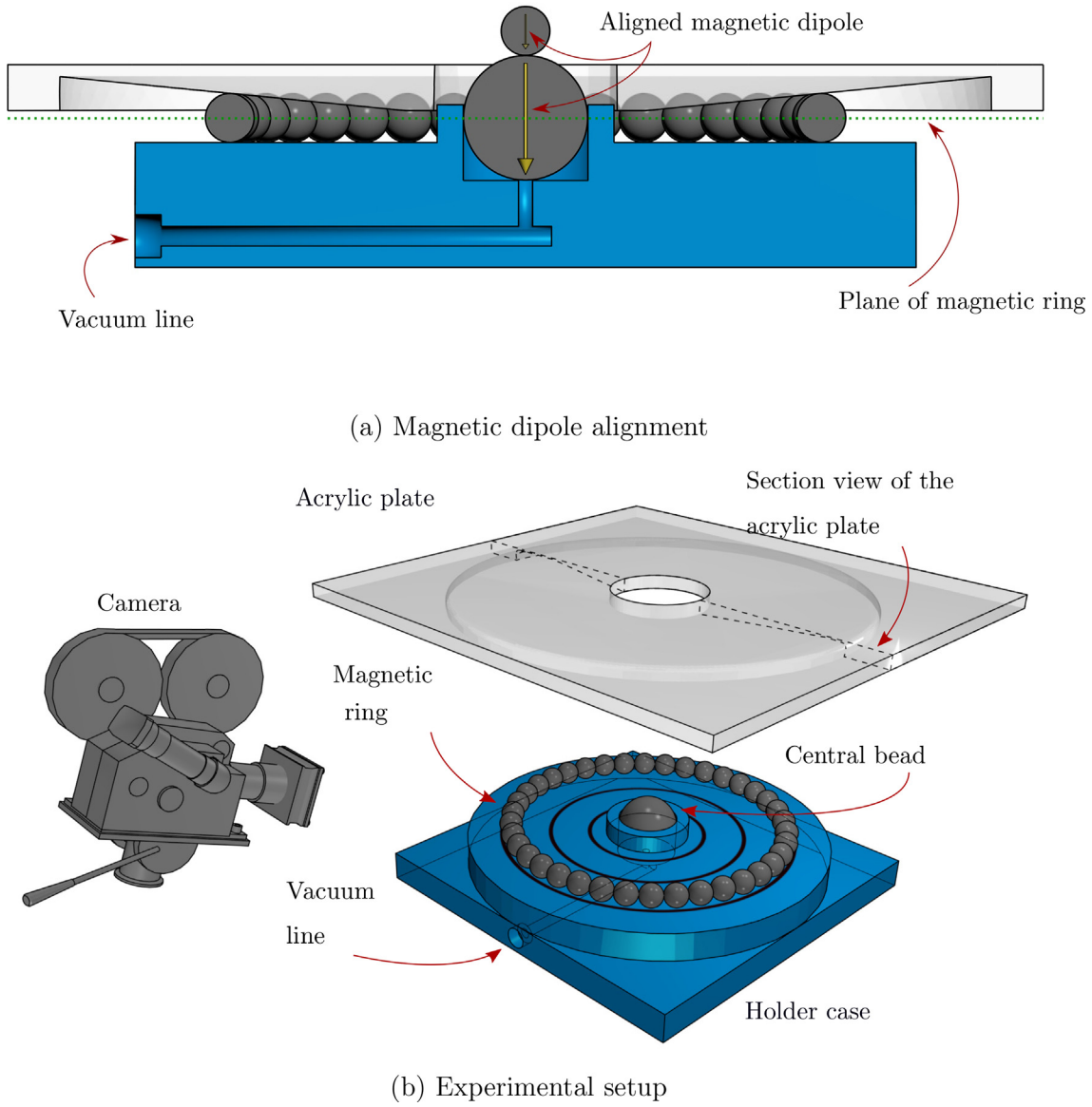

Fig. 10. (a) Alignment of the central magnetic dipole and (b) schematic view of the experimental set up to measure instability of the magnetic ring under the influence of a central magnetic dipole.

mechanical loading. There is, however, a fundamental difference between the two loadings. While the dipolar loading applied to each particle of the ring has varying magnitude and direction, depending on position and rotation of the particle , the mechanical loading has constant magnitude and always directs toward the (initial) center of the ring. This distinction leads to different instability paths for two loading cases. Specifically, in-plane instability modes always occur first for the case of compressive dipolar loading, regardless of the number of particles . This implies that it might be costly in terms of energy for the ring to deform out of its plane; instead, the ring tends to deform in its plane, subverting the circular structure of dipole moments when instability occurs. In contrast, in-plane or out-of-plane instability modes occur first for the remaining case when number of particles $N < 10$ or $N \geq 10$, respectively. Firstly, this result suggests that for sufficiently large ring sizes, the magnetic interaction between the particles of the ring dominates over the influence of the mechanical loading so that the ring tends to deform out of its plane, preserving the preferably circular arrangement of the dipole moments of the ring when instability arises. Secondly, the transition with the ring size N is reminiscent of an elastic ring with intrinsic curvature subject to an external pressure, as may be attained by a soap film spanning the ring. Previous work (Hoang and Fried, 2018) shows that elastic rings with intrinsic curvature exhibit in-plane or out-of-plane instability modes for, respectively, sufficiently small or sufficiently large ring sizes. Having obtained qualitative comparisons concerning the two loading scenarios, it would be helpful to have quantitative results. To do so, we would need to make a connection between the two loading parameters k and f. Prior to instability, each particle of the ring subject to dipolar loading experiences a dipolar force whose direction is toward the center of the ring and (dimensionless) magnitude is, from $(16)_2$ with $f = 0$ (in the absence of mechanical loading),

$$f_{\text{dipolar}} = |\frac{\partial W}{\partial \boldsymbol{r}_i}| = 15k|\frac{\mathscr{C}(\boldsymbol{r}_i)(\boldsymbol{e}_3 \otimes \boldsymbol{u}_i)}{r_i^4}| = \frac{384k^2 \sin^4 \Pi_N}{3\sigma_3 - \sigma_2}. \tag{62}$$

Substituting the numerical values k^{cr} of k at which instability occurs into the above equation, we find that $f^{\text{cr}}_{\text{dipolar}} < f^{\text{cr}}$, thus implying the magnetic ring subject to dipolar loading is less stable

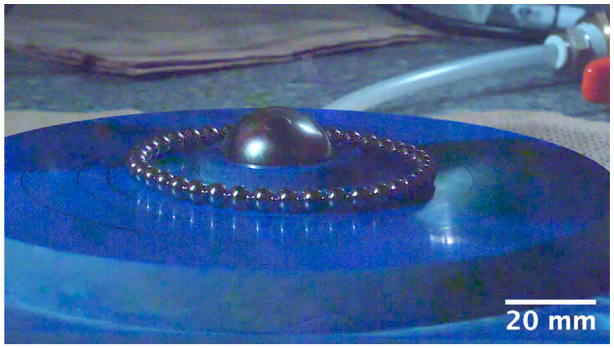

(a) 10ms

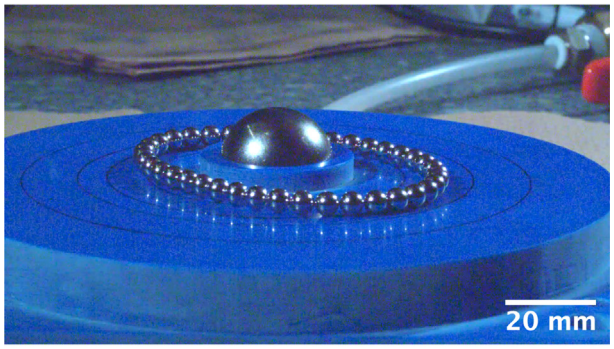

(b) 50ms

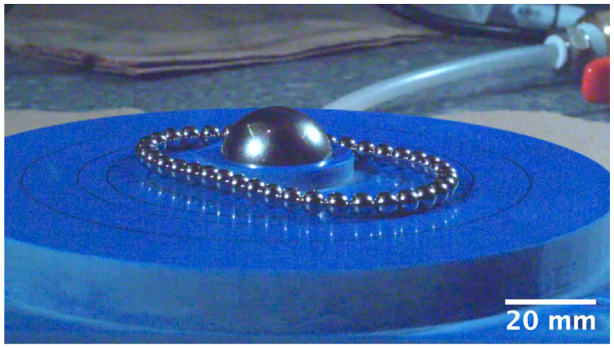

(c) 65ms

Fig. 11. Frames of the video recorded with a color-high speed camera at (a)10 ms, (b)50 ms and (c)65 ms.

than that subject to mechanical loading. This result is sensible since the magnitude of dipolar loading applied to each particle of the ring is varying and inversely proportional to the fourth power of distance of the particle (see (62)), whereas that of mechanical loading is constant. To dominant order in N as $N \to \infty$, with reference to (48) and (49), the expression (62) yields

$$f^{\mathrm{cr}}_{\mathrm{dipolar},\infty} \sim 4(z+1/6)\Pi_N^3, \qquad z \approx 1.202. \tag{63}$$

From (52) and (63), we see that, to dominant order in N, the critical value for the converted parameter $f^{\mathrm{cr}}_{\mathrm{dipolar},\infty} \approx f^{\mathrm{cr}}_{\infty}/4$. The factor 1/4 in this result poses a natural question whether a centrally directed varying mechanical loading, whose magnitude is inversely proportional to the fourth power of distance of the particle and direction is always toward the (initial) center of the ring, would cause instability at critical values determined by (63). To answer this question, we similarly draw a link of the posed problem with that of an elastic ring subject to the same loading condition, as done in Section 6.2. For an elastic ring subject to a centrally directed varying mechanical loading whose magnitude is inversely proportional to the fourth power of the distance from the application point of loading to the initial center of the elastic ring, instability occurs when dimensionless pressure $v = 1.5$ via the in-plane instability mode (Hoang, 2019). Utilizing the notion of an effective magnetic bending stiffness (Hall et al., 2013; Vella et al., 2013), we find that for the posed problem, instability occurs when, to dominant order in N as $N \to \infty$,

$$f^{\mathrm{cr}}_{\mathrm{4th\ central},\infty} \sim 6(z+1/6)\Pi_N^3, \qquad z \approx 1.202, \tag{64}$$

via the in-plane instability mode. Comparing (63) with (64), we infer that the magnetic ring subject to dipolar loading is less stable than that subject to centrally directed varying mechanical loading whose magnitude is inversely proportional to the fourth power of the distance of the particle . This result is in harmony with the fact that direction of the dipolar loading applied to each particle of the ring depends on its dipole moment or rotation of the particle whereas that of the centrally directed varying mechanical loading is always toward the (initial) center of the ring. Having quantitatively compared the two loading mechanisms, we now summarize important results as given in Table 3. For completeness, we also show instability criteria for elastic rings with no intrinsic curvature and no twist subject to traditionally considered pressure-like loadings. Since these criteria are expressed in terms of the dimensionless pressure v, we follow the established practice.

We also performed a simple experiment for the case of magnetic rings purely loaded by a central point dipole and found good agreement between theoretical predictions and experimental results. Although the instability happens very quickly (in milliseconds), we do not observe any signs of dynamic instability which appeared in a similar system of an elastic ring spanned by a soap film where higher instability modes are excited (Box et al., 2020). Since the circular arrangement of dipole moments is undermined after instability occurs in our case, the ring tends to deform in a way that alignment of the dipole moments can be achieved. We believe that the ring deforms, via the lowest mode with $q = 2$, to a preferable configuration in which a single pair of two touching magnetic chains is formed in the ring. The lengths of these chains depend on the intensity k of dipolar loading and tend to one half the length of the ring, i.e., the ring becomes a ribbon, as $k \to \infty$.

Being based on linear stability analysis, our study does not provide information on the shapes of the magnetic rings after instability occurs. Additionally, in the case of magnetic rings loaded by a central point dipole, we showed in Section 4 that along with the circular equilibrium configuration with tilted dipole moments in the ring as illustrated in Fig. 2a and studied here, there exists another circular equilibrium configuration with dipole moments in the ring antiparallel to the central point dipole. This configuration was observed in colloidal particle mixtures under the application of a magnetic field (Erb et al., 2009). For future work, it is therefore appropriate to extend our model to take into account the influence of external magnetic field and to perform comprehensive postbuckling analysis.

Declaration of Competing Interest

The authors declare that they have no known competing financial interests or personal relationships that could have appeared to influence the work reported in this paper.

Acknowledgements

The authors gratefully acknowledge support from the Okinawa Institute of Science and Technology Graduate University with

Table 3
Critical value of dimensionless pressure v at which instability occurs and corresponding instability modes for magnetic rings (the first two cases) and for elastic rings (the remaining cases). Note that for magnetic rings, the (approximated) values of v as $N \to \infty$ are given.

Loading type	Characteristics	Critical value of v	Instability mode	References
Uniform central (magnetic ring)	Constant magnitude & centrally directed	4	out-of-plane	This work
Dipolar (magnetic ring)	Varying magnitude, inversely proportional to 4th power of distance & unspecified direction	1	in-plane	This work
Uniform central (elastic ring)	Constant magnitude & centrally directed	4.5	in-plane	(Albano and Seidel, 1973; Naschie and Nashai, 1975; Sills and Budiansky, 1978) (Simitses and Hodges, 2006; Singer and Babcock, 1970; Thurston, 1989)
Uniform central (elastic ring)	Constant magnitude & centrally directed	4	out-of-plane	(Hoang, 2019)
2nd central (elastic ring)	Varying magnitude, inversely proportional to square of distance & centrally directed	2.25	in-plane	(Hoang, 2019; Sills and Budiansky, 1978; Thurston, 1989)
4th central (elastic ring)	Varying magnitude, inversely proportional to 4th power of distance & centrally directed	1.5	in-plane	(Hoang, 2019)
Dead (elastic ring)	Constant magnitude & constant direction	4	in-plane	(Naschie and Nashai, 1975; Schmidt, 1981; Simitses and Hodges, 2006; Singer and Babcock, 1970; Thurston, 1989)
Dead (elastic ring)	Constant magnitude & constant direction	3	out-of-plane	Hoang (Unpublished)
Pressure or soap film (elastic ring)	Constant magnitude & normal direction (perpendicular to ring)	3	in-plane	(Biria and Fried, 2014; Carrier, 1947; Chen and Fried, 2014; Flaherty et al., 1972) (Giomi and Mahadevan, 2012; Naschie and Nashai, 1975; Seidel and Albano, 1973; Sills and Budiansky, 1978) (Simitses and Hodges, 2006; Singer and Babcock, 1970; Tadjbakhsh and Odeh, 1967; Thurston, 1989)

subsidy funding from the Cabinet Office, Government of Japan. This research is additionally funded by Vietnam National Foundation for Science and Technology Development (NAFOSTED) under Grant No. 107.02-2020.11. The authors would like to thank Eliot Fried at Mathematics, Mechanics, and Materials Unit, Okinawa Institute of Science and Technology, Japan for insightful discussions, especially his suggestion of utilizing multipole moments to express equilibrium and stability criteria in Section 3 in compact forms and for helpful guidance on matters of grammar and style. The author would also like to thank two anonymous referees for constructive criticism and suggestions.

Appendix A

A.1. Expressions for the second-order partial derivatives at the base configuration

Substituting the circular base configuration with tilted dipole moments (27) and (29) into (21), we find that the second partial derivatives entering the double sum on the first line of stability criteria (17) can be expressed as, with $\psi_{ij} = (j-i)\Pi_N$,

$$\frac{\partial^2 V}{\partial \boldsymbol{u}_i \partial \boldsymbol{u}_j} = \frac{\sin^3 \Pi_N}{2\sin^3|\psi_{ij}|}\big((3\cos(2\psi_{ij})-1)\boldsymbol{\rho}_i\otimes\boldsymbol{\rho}_i + 3\sin(2\psi_{ij})(\boldsymbol{\rho}_i\otimes\boldsymbol{\varphi}_i + \boldsymbol{\varphi}_i\otimes\boldsymbol{\rho}_i) - (3\cos(2\psi_{ij})+1)\boldsymbol{\varphi}_i\otimes\boldsymbol{\varphi}_i + 2\boldsymbol{e}_3\otimes\boldsymbol{e}_3\big), \tag{A.1}$$

$$\begin{aligned}\frac{\partial^2 V}{\partial \boldsymbol{r}_i \partial \boldsymbol{u}_j} = \frac{3\sin^4 \Pi_N}{4\sin^5|\psi_{ij}|}\big(&\cos\theta(5\cos(2\psi_{ij})-3)\sin(2\psi_{ij})\boldsymbol{\rho}_i\otimes\boldsymbol{\rho}_i \\ &-4\sin\theta\sin^2\psi_{ij}(\boldsymbol{\rho}_i\otimes\boldsymbol{e}_3 + \boldsymbol{e}_3\otimes\boldsymbol{\rho}_i) \\ &-\cos\theta(5\cos(3\psi_{ij})+3\cos\psi_{ij})\sin\psi_{ij}\boldsymbol{\varphi}_i\otimes\boldsymbol{\varphi}_i \\ &+2\sin\theta\sin(2\psi_{ij})(\boldsymbol{\varphi}_i\otimes\boldsymbol{e}_3 + \boldsymbol{e}_3\otimes\boldsymbol{\varphi}_i) \\ &+2\cos\theta(5\cos(2\psi_{ij})+3)\sin^2\psi_{ij}(\boldsymbol{\rho}_i\otimes\boldsymbol{\varphi}_i + \boldsymbol{\varphi}_i\otimes\boldsymbol{\rho}_i) \\ &+2\cos\theta\sin(2\psi_{ij})\boldsymbol{e}_3\otimes\boldsymbol{e}_3\big),\end{aligned} \tag{A.2}$$

$$\begin{aligned}\frac{\partial^2 V}{\partial \boldsymbol{r}_i \partial \boldsymbol{r}_j} = \frac{3\sin^5 \Pi_N}{16\sin^5|\psi_{ij}|}\big(&-2((9+\cos(2\theta))\sin(2\psi_{ij}) + 5\cos^2\theta\sin(4\psi_{ij})) \\ &(\boldsymbol{\rho}_i\otimes\boldsymbol{\varphi}_i + \boldsymbol{\varphi}_i\otimes\boldsymbol{\rho}_i) - (4\cos^2\psi_{ij}(5\cos(2\psi_{ij})+1) \\ &+\cos(2\theta)(5\cos(4\psi_{ij}) + 52\cos(2\psi_{ij}) - 17))\boldsymbol{\rho}_i\otimes\boldsymbol{\rho}_i \\ &+32\sin(2\theta)\sin(2\psi_{ij})(\boldsymbol{\rho}_i\otimes\boldsymbol{e}_3 + \boldsymbol{e}_3\otimes\boldsymbol{\rho}_i) \\ &-64\sin(2\theta)\cos^2\psi_{ij}(\boldsymbol{\varphi}_i\otimes\boldsymbol{e}_3 + \boldsymbol{e}_3\otimes\boldsymbol{\varphi}_i) \\ &+(10\cos^2\theta\cos(4\psi_{ij}) + 8(3+8\cos(2\theta))\cos(2\psi_{ij}) \\ &+27\cos(2\theta)+3)\boldsymbol{\varphi}_i\otimes\boldsymbol{\varphi}_i - 4(6\cos^2\theta\cos(2\psi_{ij}) \\ &+11\cos(2\theta)-1)\boldsymbol{e}_3\otimes\boldsymbol{e}_3\big).\end{aligned} \tag{A.3}$$

Similarly, substituting the circular base configuration with tilted dipole moments (27) and (29) into (22), we find that the second partial derivatives entering the single sum on the second line of stability criteria (17) can be expressed as

$$\begin{aligned}\frac{\partial^2 E}{\partial \boldsymbol{u}_i \partial \boldsymbol{r}_i} = \sum_{\substack{1\leqslant j\leqslant N \\ j\neq i}} \frac{3\sin^4 \Pi_N}{8\sin^5|\psi_{ij}|}\big(&4\cos\theta\cos^2\psi_{ij}\sin(2\psi_{ij})\boldsymbol{\rho}_i\otimes\boldsymbol{\rho}_i - 8 \\ &\times\sin\theta\sin^2\psi_{ij}(\boldsymbol{\rho}_i\otimes\boldsymbol{e}_3 + \boldsymbol{e}_3\otimes\boldsymbol{\rho}_i) - \cos\theta(6 \\ &\times\sin(2\psi_{ij}) + \sin(4\psi_{ij}))\boldsymbol{\varphi}_i\otimes\boldsymbol{\varphi}_i + 4\sin\theta\sin(2\psi_{ij}) \\ &\times(\boldsymbol{\varphi}_i\otimes\boldsymbol{e}_3 + \boldsymbol{e}_3\otimes\boldsymbol{\varphi}_i) + 4\cos\theta(\cos(2\psi_{ij})+3) \\ &\times\sin^2\psi_{ij}(\boldsymbol{\rho}_i\otimes\boldsymbol{\varphi}_i + \boldsymbol{\varphi}_i\otimes\boldsymbol{\rho}_i) + 4\cos\theta\sin(2\psi_{ij})\boldsymbol{e}_3 \\ &\otimes\boldsymbol{e}_3) + 48k\sin^4\Pi_N(\boldsymbol{\rho}_i\otimes\boldsymbol{e}_3 + \boldsymbol{e}_3\otimes\boldsymbol{\rho}_i),\end{aligned} \tag{A.4}$$

$$\begin{aligned}\frac{\partial^2 E}{\partial \boldsymbol{r}_i^2} = &96k\sin^5\Pi_N(\sin\theta(3\boldsymbol{e}_3\otimes\boldsymbol{e}_3 + \boldsymbol{\varphi}_i\otimes\boldsymbol{\varphi}_i - 4\boldsymbol{\rho}_i\otimes\boldsymbol{\rho}_i) \\ &+\cos\theta(\boldsymbol{\varphi}_i\otimes\boldsymbol{e}_3 + \boldsymbol{e}_3\otimes\boldsymbol{\varphi}_i)) + 2f\sin\Pi_N(\boldsymbol{\varphi}_i\otimes\boldsymbol{\varphi}_i + \boldsymbol{e}_3\otimes\boldsymbol{e}_3) \\ &-\sum_{\substack{1\leqslant j\leqslant N \\ j\neq i}}\frac{\partial^2 V}{\partial \boldsymbol{r}_i\partial \boldsymbol{r}_j}.\end{aligned} \tag{A.5}$$

A.2. Elements of the symmetric matrix $\boldsymbol{H}$

Substituting (42) into (17) and referring to the quadratic form (43), we find that the elements of the upper half of the symmetric 4×4 matrix $\boldsymbol{H}$ are

$$\begin{aligned} H_{11} &= 2\sigma_3 - \sigma_2 + \ underset{}{1 \leqslant j \leqslant N} \\ &\quad - 1 \sum (1 + \sin^2 j\Pi_N)\csc^3 j\Pi_N \cos 2qj\Pi_N, \end{aligned} \tag{A.6}$$

$$\begin{aligned} H_{22} &= 2\sigma_3 - \sigma_2 + \ underset{}{1 \leqslant j \leqslant N} \\ &\quad - 1 \sum (\cos 2\theta - \sin^2\theta \cos^2 j\Pi_N)\csc^3 j\Pi_N \cos 2qj\Pi_N, \end{aligned} \tag{A.7}$$

$$\begin{aligned} H_{23} &= -6\cos\theta \sin\Pi_N (8k \cot\Pi_N + \sin\theta \ underset{}{1 \leqslant j \leqslant N} \\ &\quad -1 \sum (\cot q\Pi_N \cot j\Pi_N \sin 2qj\Pi_N + \cot q\Pi_N \cos^2 j\Pi_N (1 + \cos^2 j\Pi_N) \\ &\quad - \cot\Pi_N \cos^2 qj\Pi_N (2 + \cos^2 j\Pi_N))\csc^3 j\Pi_N), \end{aligned} \tag{A.13}$$

$$\begin{aligned} H_{24} &= -3\cos 2\theta \sin\Pi_N \ underset{}{1 \leqslant j \leqslant N} \\ &\quad - 1 \sum \cot j\Pi_N \csc^3 j\Pi_N \sin 2qj\Pi_N, \end{aligned} \tag{A.14}$$

$$\begin{aligned} H_{34} &= 6\sin^2\Pi_N (16k\cos\theta \cot q\Pi_N + \sin 2\theta \ underset{}{1 \leqslant j \leqslant N} \\ &\quad -1 \sum \left(4\cot q\Pi_N \cos^2 j\Pi_N \sin^2 qj\Pi_N - \cot\Pi_N \sin 2j\Pi_N \sin 2qj\Pi_N\right)\csc^5 j\Pi_N\Big). \end{aligned} \tag{A.15}$$

$$\begin{aligned} H_{33} &= \ underset{}{1 \leqslant j \leqslant N} - 1 \sum 3\sin^2\Pi_N \csc^5 j\Pi_N \big\{ \big((\cos^2\theta(3\cos^4 j\Pi_N + 4) - 1 + (5\cos^2\theta - 3)\cos^2 j\Pi_N\big)\cos 2qj\Pi_N \\ &\quad + \cos^2 j\Pi_N (5 - 5\cos^2\theta \cos^2 j\Pi_N - 11\cos^2\theta) + 2\cos 2\theta + 1\big)\cot^2 q\Pi_N \\ &\quad + \big(\cos^2\theta(3\cos^2 j\Pi_N + 4) - 3\big)\sin 2j\Pi_N \sin 2qj\Pi_N \cot\Pi_N \cot q\Pi_N \\ &\quad + \Big(\big(\cos^2\theta(3\cos^4 j\Pi_N - 8) - 3\cos^2 j\Pi_N + 4\big)\cos 2qj\Pi_N + \sin^2 j\Pi_N (5 - 18\cos^2\theta) \\ &\quad + 5\cos^2\theta(\sin^4 j\Pi_N + 1) - 1\Big)cot^2\Pi_N \big\} + 96k\sin\theta\sin^2\Pi_N(\cot^2 q\Pi_N - 4\cot^2\Pi_N) \\ &\quad + 2f\csc^2\Pi_N \csc^2 q\Pi_N \Big(\cos^2 q\Pi_N - \tfrac{1}{4}\csc^4\Pi_N (\cos 2\Pi_N - \cos 2q\Pi_N)^2\Big) \\ &\quad - \tfrac{3}{2}(8k\sin\theta + 2\sigma_3 - \sigma_2)\csc^2\Pi_N \csc^2 q\Pi_N (\cos 2\Pi_N - \cos 2q\Pi_N)^2, \end{aligned} \tag{A.8}$$

$$\begin{aligned} H_{44} &= 48k\sin\theta(6\sin^2\Pi_N - \sin^2 q\Pi_N) \\ &\quad + 2f\csc^2\Pi_N (1 - \csc^2\Pi_N \sin^2 q\Pi_N) \\ &\quad - 6\sin^2 q\Pi_N (2\sigma_3 - \sigma_2) + 6\sin^2\Pi_N \ underset{}{1 \leqslant j \leqslant N} \\ &\quad - 1 \sum (\cos^2\theta(3\cos^2 j\Pi_N + 4) - 3)\csc^5 j\Pi_N \sin^2 qj\Pi_N, \end{aligned} \tag{A.9}$$

$$H_{12} = \sum_{1 \leqslant j \leqslant N-1} \sin\theta \cos j\Pi_N \csc^2 j\Pi_N \sin 2qj\Pi_N, \tag{A.10}$$

$$\begin{aligned} H_{13} &= 6\cos\theta \sin\Pi_N \ underset{}{1 \leqslant j \leqslant N} \\ &\quad - 1 \sum \Big(\cot q\Pi_N (1 - \sin^2 j\Pi_N \sin^2 qj\Pi_N) \\ &\quad - \cot\Pi_N (1 - \sin^4 j\Pi_N)\Big)\csc^3 j\Pi_N, \end{aligned} \tag{A.11}$$

$$H_{14} = 6\sin\Pi_N \Big(8k - \sin\theta \ underset{}{1 \leqslant j \leqslant N - 1} \sum \csc^3 j\Pi_N \sin^2 qj\Pi_N\Big), \tag{A.12}$$

For the second mode number, namely $q = 2$, these expressions become

$$H_{11} = 3\sigma_3 - 8\sigma_2 + 8\sigma_4, \tag{A.16}$$

$$\begin{aligned} H_{22} &= 8\sigma_1(2\cos 2\theta - 1) + \sigma_2(25\sin^2\theta - 9) + 3\sigma_3 \cos^2\theta \\ &\quad + 8\sigma_4 \sin^2\theta, \end{aligned} \tag{A.17}$$

$$\begin{aligned} H_{33} &= 6\sin^2\Pi_N \Big\{ 4(3(1 - 3\cos^2\theta)\sigma_1 - 2\sin^2\theta\sigma_2 + 2\cos^2\theta\sigma_3 + 3\cos^2\theta\sigma_4)\cot^2\Pi_N \\ &\quad + 4((23\cos^2\theta - 6)\sigma_1 + (9 - 24\cos^2\theta)\sigma_2 + (7\cos^2\theta - 3)\sigma_3 - 6\cos^2\theta\sigma_4)\cot\Pi_N \cot 2\Pi_N \\ &\quad + ((12 - 56\cos^2\theta)\sigma_1 + (91\cos^2\theta - 28)\sigma_2 + (15 - 43\cos^2\theta)\sigma_3 + 12\cos^2\theta\sigma_4)\cot^2 2\Pi_N \big\} \\ &\quad + 96k\sin\theta\sin^2\Pi_N(\cot^2 2\Pi_N - 4\cot^2\Pi_N) + 2f(3\csc^2\Pi_N - 2\csc^4\Pi_N) \\ &\quad - 6(8k\sin\theta + 2\sigma_3 - \sigma_2)\sin^2 3\Pi_N \csc^2 2\Pi_N, \end{aligned} \tag{A.18}$$

$$\begin{aligned} H_{44} &= 48k\sin\theta(6\sin^2\Pi_N - \sin^2 2\Pi_N) + 2f\csc^2\Pi_N (1 - 4\cos^2\Pi_N) \\ &\quad - 6\sin^2 2\Pi_N (2\sigma_3 - \sigma_2) \\ &\quad + 24\sin^2\Pi_N (3\cos^2\theta\sigma_1 + (3 - 10\cos^2\theta)\sigma_2 \\ &\quad + (7\cos^2\theta - 3)\sigma_3), \end{aligned} \tag{A.19}$$

$$H_{12} = 4\sin\theta(-3\sigma_1 + \sigma_2 + 2\sigma_4), \tag{A.20}$$

$$\mathrm{H}_{13} = 6\cos\theta\sin\Pi_N(\cot 2\Pi_N(-4\sigma_1+\sigma_3+4\sigma_4) - \cot\Pi_N(\sigma_3-\sigma_1)), \tag{A.21}$$

$$\mathrm{H}_{14} = 24\sin\Pi_N(2k-\sin\theta(\sigma_2-\sigma_1)), \tag{A.22}$$

$$\mathrm{H}_{23} = -6\cos\theta\sin\Pi_N(8k\cot\Pi_N+\sin\theta(\cot 2\Pi_N(6\sigma_3-15\sigma_2+9\sigma_1) - \cot\Pi_N(3\sigma_3-13\sigma_2+16\sigma_1-4\sigma_4))), \tag{A.23}$$

$$\mathrm{H}_{24} = -12\cos 2\theta\sin\Pi_N(\sigma_3-3\sigma_2+2\sigma_1), \tag{A.24}$$

$$\mathrm{H}_{34} = 6\sin^2\Pi_N(16k\cos\theta\cot 2\Pi_N+\sin 2\theta(16\cot 2\Pi_N(\sigma_3 - 2\sigma_2+\sigma_1) - 8\cot\Pi_N(\sigma_3-3\sigma_2+2\sigma_1))), \tag{A.25}$$

where σ_2, σ_3 are defined as (31) while σ_1, σ_4 are given as

$$\sigma_1 = \sum_{1\leqslant j\leqslant N-1}\sin(j\Pi_N) = \cot\left(\frac{\Pi_N}{2}\right),$$
$$\sigma_4 = \sum_{1\leqslant j\leqslant N-1}\sin^3(j\Pi_N) = \frac{1}{4}\left(3\cot\left(\frac{\Pi_N}{2}\right)-\cot\left(\frac{3\Pi_N}{2}\right)\right). \tag{A.26}$$

A.3. Analytical expression for lowest critical value f^{cr} of f in the absence of a dipolar load ($k = 0$) for in-plane or out-of-plane perturbation components of positions and dipole moments

When $\beta_i = 0$ and $\zeta_i = 0, i = 1\ldots,N$, the stability condition (43) reduces to

$$\boldsymbol{u}\cdot\boldsymbol{H}\boldsymbol{u} = \begin{bmatrix}\mathrm{u}_1\\ \mathrm{u}_3\end{bmatrix}\cdot\begin{bmatrix}\mathrm{H}_{11} & \mathrm{H}_{13}\\ \mathrm{H}_{31} & \mathrm{H}_{33}\end{bmatrix}\begin{bmatrix}\mathrm{u}_1\\ \mathrm{u}_3\end{bmatrix} \geq 0. \tag{A.27}$$

At critical values f_1^{cr} of f, the determinant of $\boldsymbol{H}$ vanishes:

$$\det\boldsymbol{H} = \mathrm{H}_{13}^2 - \mathrm{H}_{11}\mathrm{H}_{33} = 0. \tag{A.28}$$

Substituting (A.16), (A.18), and (A.21) with $k = 0$ and $\theta = 0$ into (A.28) yields

$$f_1^{\mathrm{cr}} = \frac{3\sin^4\Pi_N}{2(3\sigma_3-8\sigma_2+8\sigma_4)(1+\cos(2\Pi_N))(1+3\cos(2\Pi_N))}\times \{(3\sigma_3-8\sigma_2+8\sigma_4)(9\sigma_2-48\sigma_1+24\sigma_4+8(5\sigma_1-14\sigma_2+6\sigma_3)\cos(2\Pi_N)+(7\sigma_2-12\sigma_3)\cos(4\Pi_N)) - 12((4\sigma_1-\sigma_3-4\sigma_4)\cos(2\Pi_N)-4(\sigma_1+2\sigma_2-\sigma_3-2\sigma_4)\cos^2\Pi_N)^2\}. \tag{A.29}$$

When $\alpha_i = 0, \chi_i = 0$, and $\upsilon_i = 0, i = 1\ldots,N$, the stability condition (43) reduces to

$$\boldsymbol{u}\cdot\boldsymbol{H}\boldsymbol{u} = \begin{bmatrix}\mathrm{u}_2\\ \mathrm{u}_4\end{bmatrix}\cdot\begin{bmatrix}\mathrm{H}_{22} & \mathrm{H}_{24}\\ \mathrm{H}_{42} & \mathrm{H}_{44}\end{bmatrix}\begin{bmatrix}\mathrm{u}_2\\ \mathrm{u}_4\end{bmatrix} \geq 0. \tag{A.30}$$

At critical values f_2^{cr} of f, the determinant of $\boldsymbol{H}$ vanishes or

$$\det\boldsymbol{H} = \mathrm{H}_{24}^2 - \mathrm{H}_{22}\mathrm{H}_{44} = 0. \tag{A.31}$$

Substituting (A.17), (A.19), and (A.24) with $k = 0$ and $\theta = 0$ into (A.31) yields

$$f_2^{\mathrm{cr}} = 12\sin^4\Pi_N\frac{6(\sigma_3-3\sigma_2+2\sigma_1)^2-(3\sigma_3-9\sigma_2+8\sigma_1)(4\sigma_3-7\sigma_2+3\sigma_1-(2\sigma_3-\sigma_2)\cos^2\Pi_N)}{(3\sigma_3-9\sigma_2+8\sigma_1)(1-4\cos^2\Pi_N)}. \tag{A.32}$$

Appendix B. Supplementary data

Supplementary data associated with this article can be found, in the online version, at https://doi.org/10.1016/j.ijsolstr.2021.111060.

References

Albano, E.D., Seidel, P., 1973. Bifurcation of rings under concentrated centrally directed loads. ASME Journal on Applied Mechanics 40 (2), 553–558.

Avriel, M., 1976. Nonlinear Programming: Analysis and Methods. Prentice-Hall Inc.

Biria, A., Fried, E., 2014. Buckling of a soap film spanning a flexible loop resistant to bending and twisting. Proceedings of the Royal Society of London Series A, Mathematical, Physical and Engineering Sciences, 470 (2172).

Boisson, J., Rouby, C., Lee, J., Doare, O., 2015. Dynamics of a chain of permanent magnets. Europhysics Letters 109, 34002.

Box, F., Kodio, O., OâĂŹKiely, D., Cantelli, V., Goriely, A., Vella, D., 2020. Dynamic buckling of an elastic ring in a soap film. Physical Review Letters 124, 198003.

Carrier, G., 1947. On the buckling of elastic rings. Journal of Applied Mathematics and Physics 26, 94–103.

Chen, Y.-C., Fried, E., 2014. Stability and bifurcation of a soap film spanning a flexible loop. Journal of Elasticity 116 (1), 75–100.

Danilov, V., Prokopyeva, T., Kantorovich, S., 2012. Ground-state structures and structural transitions in a monolayer of magnetic dipolar particles in the presence of an external magnetic field. Physical Review E 86 (061408).

Erb, R.M., Son, H.S., Samanta, B., Rotello, V.M., Yellen, B.B., 2009. Magnetic assembly of colloidal superstructures with multipole symmetry. Nature 457 (19), 999–1002.

Flaherty, J.E., Keller, J.B., Rubinow, S.I., 1972. Post buckling behavior of elastic tubes and rings with opposite sides in contact. SIAM Journal on Applied Mathematics 23, 446–455.

Giomi, L., Mahadevan, L., 2012. Minimal surfaces bounded by elastic lines. Proceedings of the Royal Society of London Series A, Mathematical, Physical and Engineering Sciences 468, 1851–1864.

Hall, C.L., Vella, D., Goriely, A., 2013. The mechanics of a chain or ring of spherical magnets. SIAM Journal on Applied Mathematics 73, 2029–2054.

Hoang, T.M., 2019. Influence of chirality on buckling and initial postbuckling of inextensible rings subject to central loadings. International Journal of Solids and Structures 172–173, 97–109.

Hoang, T.M., Fried, E., 2018. Influence of a spanning liquid film on the stability and buckling of a circular loop with intrinsic curvature or intrinsic twist density. Mathematics and Mechanics of Solids 23 (1), 43–66.

Hu, N., Burgueno, R., 2015. Buckling-induced smart applications: recent advances and trends. Smart Materials and Structures 24, 063001.

Jackson, J.D., 1999. Classical Electrodynamics. Wiley, New York, NY.

Jund, P., Kim, S., Tománek, D., Hetherington, J., 1995. Stability and fragmentation of complex structures in ferrofluids. Physical Review Letters 74 (15), 3049–3052.

Kun, F., Pál, K.F., Wen, W., Tu, K.N., 2000. Break-up of dipolar rings under an external magnetic field. Physics Letter A 277, 287–293.

Kun, F., Wen, W., Pál, K.F., Tu, K.N., 2001. Breakup of dipolar rings under a perpendicular magnetic field. Physical Review E 64, 061503-1–061503-8..

Martinez-Pedrero, F., Cebers, A., Tierno, P., 2016. Dipolar rings of microscopic ellipsoids: Magnetic manipulation and cell entrapment. Physical Review Applied 6, 034002.

Naschie, M.E., Nashai, A.E., 1975. Influence of loading behavior on the post buckling of circular rings. AIAA Journal 14 (2).

Prokopieva, T.A., Danilov, V.A., Kantorovich, S.S., Holm, C., 2009. Ground state structures in ferrofluid monolayers. Physical Review E 80, 031404.

Schmidt, R., 1981. In-plane postbuckling of rings subjected to a constant-directional pressure load. Journal of Applied Mathematics and Physics 32, 616–619.

Schönke, J., Fried, E., 2017. Stability of vertical magnetic chains. Proceedings of the Royal Society A, Mathematical, Physical and Engineering Sciences 473, 20160703.
Seidel, P., Albano, E.D., 1973. Bifurcation of circular rings under normal concentrated loads. ASME Journal on Applied Mechanics 40 (1), 233–238.
Sills, L., Budiansky, B., 1978. Postbuckling ring analysis. ASME Journal on Applied Mechanics 45 (1), 208–210.
Simitses, G.J., Hodges, D.H., 2006. Fundamentals of Structural Stability. Butterworth-Heinemann.
Singamaneni, S., Bliznyuk, V.N., Binek, C., Tsymbal, E.Y., 2011. Magnetic nanoparticles: recent advances in synthesis, self-assembly and applications. Journal Materials Chemistry 21, 16819.
Singer, J., Babcock, C.D., 1970. On the buckling of rings under constant directional and centrally directed pressure. Journal of Applied Mechanics 37 (1), 215–218.
Tadjbakhsh, I., Odeh, F., 1967. Equilibrium states of elastic rings. Journal of Mathematical Analysis and Applications 18, 59–74.
Thurston, G.A., 1989. Application of newton's method to postbuckling of rings under pressure loadings. NASA Technical paper.
van Putten, M.H., 2017. Introduction to Methods of Approximation in Physics and Astronomy. Springer Nature Singapore Pte Ltd.
Vanderbei, R.J., Kolemen, E., 2007. Linear stability of ring systems. The Astronomical Journal 133, 656–664.
Vella, D., Pontavice, E., Hall, C.L., Goriely, A., 2013. The magneto-elastica: from self-buckling to self-assembly. Proceedings of the Royal Society A 470, 20130609.
Wei, A., Tripp, S.L., Liu, J., Kasama, T., Dunin-Borkowski, R.E., 2009. Calixarene-stabilised cobalt nanoparticle rings: Self-assembly and collective magnetic properties. Supramolecular Chemistry 21 (3–4), 189–195.
Wen, W., Kun, F., Pál, K.F., Zheng, D.W., Tu, K.N., 1999. Aggregation kinetics and stability of structures formed by magnetic microspheres. Physical Review E 59 (5), 4758–4761.